

A System Level FMCW RADAR Optimization For Automotive Powertrain Control Application Requirements

by

Christopher Beg

A thesis
presented to the University of Waterloo
in fulfillment of the
thesis requirement for the degree of
Master of Applied Science
in
Electrical and Computer Engineering

Waterloo, Ontario, Canada, 2013

© Christopher Beg 2013

I hereby declare that I am the sole author of this thesis. This is a true copy of the thesis, including any required final revisions, as accepted by my examiners.

I understand that my thesis may be made electronically available to the public.

Abstract

A full system level analysis, design, and realization of frequency-modulation / continuous-wave (FMCW) RADAR is presented in this thesis. RADAR technology has been around for over half a century, and has found itself in a wide range of applications effecting every day life. As such, there are many possible system level tradeoffs that can be made when designing a sensor for a specific application. This paper will focus on designing a sensor for a hybrid electric vehicle powertrain control unit, as part of a new application in fuel economy improvement. The system level analysis will derive a full baseband signal analysis model, and examine some of the commonly used modulation schemes. Next, a method for tuning the modulation waveform properties to optimize the sensor specifically for the application requirements is presented. Finally a system level realization is proposed to produce synchronous and streamlined processing of the signals, while providing flexibility to tune the implementation as suggested during the modulation waveform optimization.

As a proof of concept, a hardware prototyping platform was designed and built to allow acquisition of real signals which are to be fed into a signal processing algorithm. The signal processing algorithm to decode the measurement results can then be developed effectively using real data. Some of the measurement results obtained with the prototyping platform and system optimizations suggested within this thesis are presented to verify the analysis and modeling performed.

Acknowledgements

I would like to thank all the little people who made this possible. I would also like to acknowledge the Natural Sciences and Engineering Research Council (NSERC) of Canada for their funding and inspiring innovation.

Table of Contents

List of Tables	viii
List of Figures	ix
1 Introduction	1
1.1 Designing To Meet Requirements	1
1.2 Motivation	1
1.3 Prior Art	3
1.4 Contributions	4
2 RADAR Background	5
2.1 Measurements Using Radio Waves	5
2.2 General Performance Limitations	7
2.3 The FMCW System	10
2.4 Mathematical Theory of FMCW	12
2.4.1 The RF Front End	12
2.4.2 Combined System Theory	15
2.5 The FMCW Modulating Waveform	19
2.5.1 Sawtooth Modulation	19
2.5.2 Triangular Modulation	24
2.5.3 Sinusoidal Modulation	29

3	Baseband and Processing Optimization	33
3.1	Introduction to simplifications	34
3.2	Combining Theory with Signal Processing	36
4	Prototyping Platform and System Realization	41
4.1	Introduction	41
4.2	A RADAR Prototyping Platform	42
4.2.1	Platform Requirements	42
4.2.2	Hardware	43
4.2.3	Software	45
4.2.4	Final Platform	47
4.3	Realization of Baseband Optimizations	48
4.4	Realization Requirements	49
4.5	Design Realization	50
5	Field and Lab Measurement Results	54
5.1	Verification	54
5.2	System Setup	55
5.3	Lab Measurements of System Setup	58
5.4	Theoretical Analysis of Expected Results	61
5.5	Field Measurements System	63
6	Conclusions	66
6.1	Modulation Waveform Comparison	66
6.2	Baseband Optimizations	67
6.3	Realization	67
6.4	Prototyping Platform	67
6.5	Future Work	68

References	69
APPENDICES	71
A Prototyping Platform Schematics and Layout	72
B Prototyping Platform Communication DLL Interface	86
C Matlab DLL Wrapper Functions	87
Glossary	95

List of Tables

3.1	System Specifications	37
3.2	N vs Fs and Processing Cost tradeoff	38
3.3	System Tuned Parameters	40
5.1	System Tuning Specifications and Requirements	57
5.2	System Tuning Realization Parameters	58

List of Figures

2.1	FMCW Top Level System Diagram	11
2.2	FMCW RF Front End System Diagram	13
2.3	Sawtooth Modulation Waveform Overview	20
2.4	Sawtooth Modulation Frequency Difference	23
2.5	Triangle Modulation Waveforms	25
2.6	Triangular Modulation Frequency Difference	28
2.7	Sinusoidal Modulation Waveforms	30
2.8	FMCW Sinusoid Modulation Frequency vs Time	32
3.1	FMCW Triangle Modulation Output Frequency vs Time	35
3.2	Fs and Processing Cost vs N	39
4.1	System Block Diagram	42
4.2	Prototyping Platform With RF Module	48
4.3	Top level architecture	49
4.4	Resulting waveform and timing	50
4.5	Analog and digital front end	51
4.6	Waveform generator block	52
4.7	Sample Collection	52
5.1	RFBeam K-MC4 Module VCO Tuning	55
5.2	RF Measurements	56

5.3	ADC Clock (4x clock)	59
5.4	Modulating Waveform Up-Chirp Period	59
5.5	Modulating Waveform Down-Chirp Period	60
5.6	Modulating Waveform Amplitude	60
5.7	40m theoretical result	61
5.8	80m theoretical result	62
5.9	40m measurement	63
5.10	80m measurement	64

Chapter 1

Introduction

1.1 Designing To Meet Requirements

This thesis examines an analysis based procedure for which to obtain a low cost and low complexity [RADAR](#) measurement system. The procedure aims to meet application specific requirements by making tradeoffs and optimizations at the system level.

1.2 Motivation

The main motivation for producing a low cost and low complexity system spans many use-cases. The primary use-case which inspired the work and analysis to be conducted in the direction presented within this thesis has been focused on automotive power-train control systems.

As the automotive industry strives to meet consumer and global demand to improve fuel efficiency and reduce emissions, the vehicles of tomorrow are becoming smarter and will require more advanced sensory data to realize the control systems. One direction which may bring promise to achieving a more energy efficient mode of transportation is the electric or the hybrid-electric power-train. Companies such as Tesla Motors have been investing a great deal of resources and expertise into this very area. As these emerging technologies start to become more feasible and publicly accepted, more opportunity is created to leverage further potential by designing "smarter" control systems.

With a traditional hydrocarbon combustion based power-train, energy stored in the chemical bonds of the fuel is transformed into mechanical or kinetic energy. Through the

process of this conversion, the majority of the energy is lost in the form of heat, friction, or noise. Additionally, energy will be lost while the vehicle is at an intersection idling. This makes such a power-train inefficient from an energy conversion point of view. In addition, once the energy is released from the chemical bonds, the process cannot be reversed to transfer kinetic energy back into a reusable energy form. This means after a vehicle accelerates to a target cruising velocity, the deceleration or braking process works by transferring the kinetic energy into heat or thermal energy by generating friction between the brake-pad and rotor/drum resulting in loss.

With an electric power-train, electric energy is transferred from electro-chemical sources such as lithium-ion or nickel-metal-hydride batteries into kinetic through magnetic field based electric motors. Switch-mode power converter systems can facilitate the transfer of power from the potential stored within a battery to the motor or load. With fewer mechanical components, and no necessity for the motor to always idle, the energy loss due to inefficiencies are dependent on non-ideal characteristics of the power converter such as switch resistance, wire impedance, and passive component losses. Further more, one big advantage to an electric power-train over a combustion power-train is the ability to transfer kinetic energy back into electric potential energy and store it back in the battery for future use. This is accomplished within the power converter by changing the direction of power transfer to move power from the motor into the battery. This essentially causes the motor to act as a generator, and such can be done to perform deceleration or braking. While operating in this mode, the kinetic energy will provide the force needed to turn the motor (generator), and will begin charging the battery.

A hybrid-electric power-train operates in a similar fashion to a pure electric power-train. However, to increase the range of the vehicle, due to limitations on current battery technologies, it is more efficient to store potential energy in the chemical form as a hydrocarbon fuel rather than as an electric-chemical form within a battery. A hybrid-electric power-train works by using a small combustion engine to run a generator and maintain sufficient charge in the battery to power the electric power-train. This has the advantage that the combustion engine can operate the generator to charge the batteries to supplement the energy stored in the battery and increase the total energy capacity. In addition, the electric power-train still has the ability to recover some of the kinetic energy through braking, and a smaller more efficiently tuned engine can be used to run the generator. This engine will be running at a constant speed, and will not be subjected to energy loss while idling.

To take full advantage of a hybrid electric powertrain, the development of a control strategy to optimize the energy flow between the two propulsion systems is a key requirement. To develop an optimal power management strategy for HEVs, one needs prior

knowledge on the entire driving cycle and future vehicle speeds. The required data related to the future driving conditions, such as velocity limitations, road grade, traffic flow, road curvature, stop points, and traffic lights may be predicted and estimated using vehicle on-board devices and sensors. The traffic speed profile in front of the vehicle is one of the most effective factors affecting the vehicle speed. In an online power management system, the optimal energy flow is computed based on the predicted velocity, driver command and route data information. The information containing upcoming traffic speed is divided into short range and long range data, which can be provided by a RADAR sensor and a vehicle-to-infrastructure communication system respectively. A RADAR sensor can be employed as an on-board sensor to provide the power management system of a HEV with the required close-range data through monitoring the area around the vehicle. Compared with laser or vision-based sensor systems, a RADAR sensor is capable of detecting targets effectively in a wide range of environmental and weather conditions with rain, snow or fog.

One of the main challenges which is addressed in this thesis is how to optimize a RADAR system to minimize cost and complexity while achieving the desired functionality. Since the primary objective of such an application specific RADAR system is to be used to improve energy efficiency, there are less constraints on accuracy and precision because the output data is not being used to impact passenger safety. When designing such a system, there is a great deal of potential to examine tradeoffs which may reduce complexity and cost when examining the design at the system level. It is the goal of this thesis to analyze the system constraints and develop a tuning procedure based on the requirements to design a system not only for automotive applications, but potentially any other application that desires to obtain an optimal system.

1.3 Prior Art

Research in RADAR systems is ongoing, specifically for automotive applications. The targeted applications range from adaptive cruise control, collision warning system, and collision avoidance, parking aid, and many other applications to improve passenger comfort [1, p.871 - p.876]. Based on the precision accuracy, and range requirements dictated by the application, both 24 GHz and 77 GHz systems are considered and deployed [2, p251 - p254].

Modern research is focused on almost every aspect of the system, ranging from antenna design to signal processing. The focus of research is performed in cost reduction, size reduction, and improved accuracy. As shown in [3], there is active work in the area of antenna design in RADAR applications. The challenge driving the research is to obtain an

antenna with a balanced tradeoff between main beam width, and side lobe level. Having a good antenna is important for RADAR applications because it will impact sensitivity, required transmit power levels, and accuracy of detection. The approach taken by [3] is to use an antenna array, which creates a single antenna out of the combination of multiple antennas.

As shown in [4], [5], and [6], many different ideas are being put forward in examining different signal processing techniques to improve detection and reduce measurement error. These ideas combine communication system and signal processing theory to develop a robust and accurate means to extract object distance and velocity information from a RADAR signal.

Another interesting area of ongoing research and experimentation is in the creation of a modulating waveform for the RADAR system. An example is presented in [7]. By creating different modulating waveforms, the distance and velocity information may be encoded slightly different (i.e., frequency, phase, amplitude). By examining different waveform types, a system to process and extract the desired information can be designed, which may allow for simplified processing, higher sensitivity, or faster measurement time.

1.4 Contributions

The contributions of this work has resulted in a piece to a larger project. As described in the Motivation section, a new application involving hybrid powertrain control is being developed at the University of Waterloo under Dr. Nasser Lashgarian Azad. Part of this project requires the ability for the vehicle to detect and predict future driving conditions, and is done through detecting near by object relative distance and velocity information.

To make such a sensor appealing for use on all automobiles, it will have to be low cost, low complexity, and add low overhead to the vehicle. In addition, when examining the requirements of this application, it is evident that there are many different tradeoffs which can be made to help achieve the desired goals of cost, complexity, and overhead. To balance the requirements, it is possible to do things like reduce the accuracy or reduce the time it takes to perform a measurement while still meet the overall system expectations.

The contributions described within this thesis provides an analysis and model of the baseband signal. From the model, different modulation schemes are examined. Next, a procedure to optimize the baseband signal processing is described, followed by a realization. Finally, verification of the theory was completed through developing a prototyping platform, where the system realization was implemented and tested.

Chapter 2

RADAR Background

2.1 Measurements Using Radio Waves

To perform any type of measurement, a comparison must be made to a reference, and the measurement result must be expressed as a multiple of the reference. For example, to measure a quantity of elapsed time, the International System of Units (SI) has developed a standard base unit of reference called a second. A minute is defined a multiple of 60 seconds, and an hour is defined as a multiple of 60 minutes, or 3,600 seconds. The second can also be divided to provide a finer resolution (i.e., a millisecond is 0.001 seconds), but still remains relative to the base unit of reference.

The same applies for measuring distance. The SI unit of reference for distance is defined as the meter. As of 1983, the meter was officially defined as the speed of light in a vacuum, satisfying the relationship that light travels at a constant rate of 299,792,458 meters in one second. This is given the symbol c . Therefore, one meter is equal to the distance light travels in $\frac{1}{299792458}$ (or $\frac{1}{c}$) seconds.

There are two properties which allow for measurements being performed using radio (or more precisely EM) waves. The first property is an EM wave propagates through a medium at a constant velocity. The second effect is when the wave interacts with another object, it will induce a current and result in a portion of energy being scattered back to the source. By combining these two properties, if one can measure the time it takes for a transmitted EM wave to propagate to an object, and reflect back to the point of origin, it is then possible to determine the distance. This is described in [8].

Assuming a vacuum, the wave travels at the speed of light from the source to the object, reflects, and then travels from the object back to the source at the same velocity.

This means from the time interval (Δt) between transmitting the wave and detecting the reflection, the wave has traveled 2· the distance (Δd) between the source and the object. Still assuming that the measurement is performed in a vacuum, by using the definition of the meter the distance can be calculated given by equation 2.1.

$$\Delta d = \frac{\Delta t \cdot c}{2} \quad (2.1)$$

Additionally, one important phenomenon which must be taken into account is the **Doppler** effect. During the propagation of an EM wave, the frequency will remain constant. The scattered component of the wave will also maintain a constant frequency if the object is stationary. However, if there is a relative velocity between the object and the RADAR, then a Doppler shift will result in a change in frequency. This change in frequency $f_{doppler}$ is given by equation 2.2 given a relative velocity of ΔV and a original frequency of f_o . Note that the effect is multiplied by 2, because the effect occurs twice (once during the transmission, and once during the reflection).

$$f_{doppler}(f_o) = \frac{2\Delta V}{c} f_o \quad (2.2)$$

In a medium other than a vacuum, light does not travel at the speed given by c . As simplified in [9, ch.2] and displayed in 2.3a to 2.3b, Maxwell's equations form the basis of electromagnetic wave propagation through any medium. The velocity propagation for an EM wave is determined from the wave equation, and is a function of the permittivity (ϵ), and permeability (μ), as shown in general equation 2.3a. In a vacuum, the permittivity is defined as ϵ_o , and the permeability is defined as μ_o , which will result in the wave propagating at the speed of light as shown in equation 2.3b. Both variables ϵ_o and μ_o are defined constants where $\epsilon_o \approx 8.854187817620 \cdot 10^{-12} F/m$, and $\mu_o = 4\pi \cdot 10^{-7} H/m$. To calculate the velocity within a medium, the relative permittivity (ϵ_r) and relative permeability (μ_r) is required, and may be used as shown in equation 2.3c. When air is the medium, $\epsilon_{r-air} \approx 1.0006$, and $\mu_{r-air} \approx 1.00000037$. Note that these values may vary with other factors such as temperature and frequency.

$$v = \frac{1}{\sqrt{\epsilon \mu}} \quad (2.3a)$$

$$c = \frac{1}{\sqrt{\epsilon_o \mu_o}} \quad (2.3b)$$

$$v(\varepsilon_r, \mu_r) = \frac{1}{\sqrt{\varepsilon_r \varepsilon_o} \cdot \sqrt{\mu_r \mu_o}} \quad (2.3c)$$

Given the results in equations 2.3a to 2.3c, equation 2.1 and equation 2.2 can be corrected to generalize for the propagation velocity in different mediums. The corrections for different mediums are derived in equations 2.4a and 2.4b respectively. For use in later calculations, a quantity $f_{dfactor}$ is defined in equation 2.4c as a multiplication factor which follows the relationship $f_{doppler}(f_o, \varepsilon_r, \mu_r) = f_{dfactor} \cdot f_o$.

$$\Delta d(\varepsilon_r, \mu_r) = \frac{\Delta t \cdot c}{2\sqrt{\varepsilon_r \mu_r}} \quad (2.4a)$$

$$f_{doppler}(f_o, \varepsilon_r, \mu_r) = \frac{2\Delta V}{c} \sqrt{\varepsilon_r \mu_r} f_o \quad (2.4b)$$

$$f_{dfactor} = \frac{2\Delta V}{c} \sqrt{\varepsilon_r \mu_r} \quad (2.4c)$$

In a practical system, it is fairly difficult to directly measure the amount of time required between transmitting and detecting the reflection and obtain a great deal of precision. To transform the theory into a more realistic and realizable form, a simple system will be described in section 2.4.1. Such a system measures the time indirectly through a mathematical means. Through some process, a time-stamp or a marker which can be used for synchronization is encoded into a transmitted signal, and then extracted from the received waveform through some decoding process.

Alternatively, it is relatively easy to measure a change in frequency such as a change due to a Doppler shift. This makes a system fairly capable of measuring the Doppler effect and determining the relative velocity between the object and RADAR. Such systems simply transmit a signal at a fixed frequency, detect the frequency of the scattered wave, and then determine the relative velocity using equation 2.2. Such a system is called a Doppler RADAR.

2.2 General Performance Limitations

Before going into the higher level system design, it is good to know which lower level parameters will effect and ultimately limit the performance of any RADAR sensor. A

prediction of the maximum detectable range has been derived and presented in [8, ch.2], which takes into account the physical properties of the object, antenna, and power. This is known as the range equation, and is shown in equation 2.5a. The range equation does not predict the performance to a high accuracy, but provides an optimistic first order prediction.

$$R_{max} = \left[\frac{P_t G A_e \sigma}{(4\pi)^2 S_{min}} \right]^{\frac{1}{4}} \quad (2.5a)$$

where R_{max} is the maximum range, P_t is the transmitted power, G is the antenna gain, A_e is the antenna effective aperture in m^2 , σ is the target cross section in m^2 , and S_{min} is the minimum detectable signal in Watts.

In some way, all of the above parameters can be tuned by the designer, aside from the target cross section. This equation essentially states the tradeoff between distance, power, gain, and size. One way to interpret the relationship is as the required range increases, you will require a either higher transmission power, a larger antenna gain (a narrow / focused beam), a large antenna to collect the returned signal energy, or a more sensitive receiver.

Transmitted Power

As described in [8, ch.2.9], the transmitted power is defined as the power averaged over a period of the carrier during the maximum power transmission. This quantity is generally controllable by the design of the PA (Power Amplifier). Various tradeoffs are possible when selecting an architecture or design for this component, such as efficiency, available power, and available physical size. Generally, communication systems are power limited due to the available power source (i.e., a battery or other limited source).

Antenna Gain

The majority of RADARs use a directive antenna for transmission and reception. This is because it allows for a more precise or finer beam to be received, hence increasing the resolution. The antenna gain is a measure of the power density in a particular direction given a specific antenna design, relative to the power density in the same direction if using an omnidirectional antenna with a 100 % efficiency. As derived by [8, p.54], the antenna gain is given by equation 2.6. Since the gain is a function of direction, the definition of

antenna gain refers to the maximum obtainable gain. It is assumed that the antenna for a RADAR application will be positioned such that the highest gain component is used.

$$G(\theta, \phi) = \frac{\text{Power density given azimuth } \theta \text{ and elevation } \phi}{\text{Power delivered to antenna} / (4\pi)} \quad (2.6)$$

Antenna Effective Aperture

The maximum gain of any antenna is also related to its physical area or aperture. The effective aperture is simply the product of the efficiency and the area of the antenna as shown in equation 2.7:

$$A_e = \rho A \quad (2.7)$$

where A_e is the antenna effective aperture, ρ is the antenna efficiency, and A is the antenna physical area.

Target Cross Section

The target cross section also plays an important role in estimating the performance of a system. The cross section of a target is a modeled area which is proportional to the amount of power returned, assuming that the transmitted power equally scatters in all possible directions when coming in contact with the objects surface. As described in [8, p.33], the cross section of a target may be calculated as shown in equation 2.8:

$$\sigma = \frac{\frac{\text{power scattered towards source}}{\text{unit solid angle}}}{\frac{\text{incident power density}}{4\pi}} = \lim_{R \rightarrow \infty} 4\pi R^2 \left| \frac{E_s}{E_i} \right|^2 \quad (2.8)$$

where R is the distance to target, E_s is scattered field strength, and E_i is the incident field strength.

In theory, the actual cross section of an object may be calculated by solving Maxwell's equations with the proper boundary conditions, however aside from very simple shapes this becomes extremely complex.

Minimum Detectable Signal

The receiver sensitivity can be thought of as the ability of the receiver to detect a weak signal with high probability. The higher the probability for a given signal power, or the lower detectable power for a given probability represents an increased sensitivity. The ability to detect a weak signal is generally limited by the noise energy which is present within the same spectrum as the signal. This noise may come from various sources, some which can be controlled, and others which can not. An example of a controllable source is the noise introduced by the [LNA](#) and receiver signal chain.

Based on the desired application, a probability of detection (or error rate) will drive the requirements for the minimum detectable signal. Some applications can function with higher error (or uncertainty) than others. For example, a cruise control application where distances are large may allow for higher error rate than a parking assist where distances are small. Additionally, the system may need to function in a low noise environment with high power levels, or maybe a high noise environment with low power levels. Based on the criteria of the system, the application, and the expected performance, a signal-to-noise ratio can be obtained and resulting noise figures of the system can be calculated.

Tradeoffs within the design may be made to reduce the noise, but may come at the expense of increased power consumption. An example of a non controllable source is the noise introduced through the environment. This can include sources such as atmospheric, multiple signals due to scattering, or additional transmitters within the same range. Filtering may help, however an ideal filter will only be able to remove noise from sources outside the desired signal band. To achieve the desirable performance, all of the tradeoffs will have to be weighed and assessed during the design of the various blocks.

2.3 The FMCW System

One [RADAR](#) architecture in the same class as the [Doppler](#) RADAR is the [FMCW](#), or Frequency Modulation Continuous Wave architecture. Similar to the Doppler in the sense it relies on the Doppler frequency shift principle to measure velocity, the FMCW is also able to measure distances of fixed objects which do not create a Doppler shift. This is because the FMCW architecture creates a frequency shift proportional to distance in addition to the Doppler shift.

The FMCW RADAR system has the advantage over more advanced systems such as Coded RADAR or Ultra-Wide-Band RADAR in the sense that it is simple, low cost, and

widely available. On the down side, FMCW RADAR systems are subjective to jamming or interference from other systems, which places the problem of handling a multi-system environment with the baseband controller.

From a system perspective, an FMCW RADAR consists of four main components. The main components are illustrated in figure 2.1 and listed as follows:

- An RF front end consisting of all RF subsystem components
- A VCO tuning voltage generator for producing a FM signal
- An ADC for digitizing the information signal
- A processor for performing all baseband control and processing

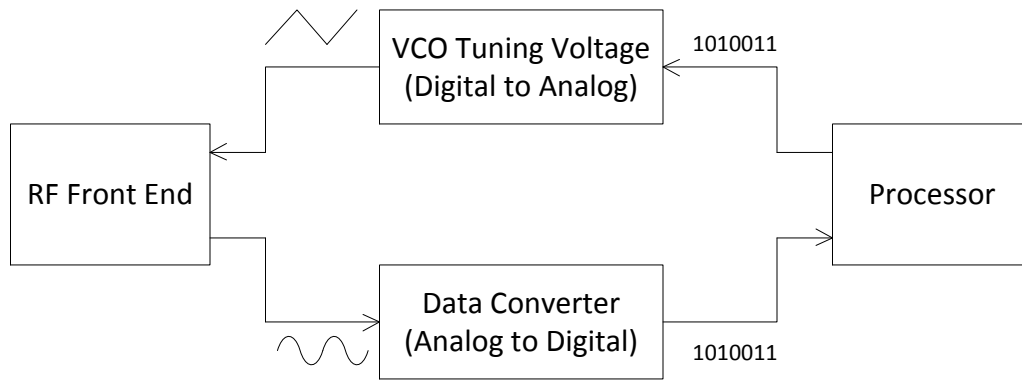


Figure 2.1: FMCW Top Level System Diagram

An FMCW system is a direct FM modulation system, where the modulating signal directly controls a voltage-controlled-oscillator (VCO) tuning voltage. The prototype function for a FM signal is given by equation 2.9. The VCO output frequency is then proportional to the tuning voltage.

$$f(t) = A_o \sin \left(2\pi f_c t + \beta \int_{-\infty}^t V_{tune}(\tau) d\tau \right) \quad (2.9)$$

It is through the VCO tuning voltage which the transmitted RF signal is created. For reasons described in section 2.4 below, the tuning voltage waveform usually takes on a

sinusoid, sawtooth or a triangular shape This is the input to the RF front end. As with any wideband FM system, the frequency domain representation of the transmitted signal will have infinite sidebands, and hence by definition will have an infinite bandwidth (described in more detail in section 2.4). For practical analysis of FM bandwidth, a generally accepted rule of thumb follows Carson’s bandwidth rule, which approximates the bandwidth of which 98 percent of energy is contained. It is through this evaluation that the transmitted bandwidth can be evaluated.

The output of the RF front end in an FMCW system is a sinusoidal waveform with the distance and velocity information encoded within the frequency. It is possible for more advanced multi-channel FMCW systems to extract not only distance and velocity magnitude information, but also obtain an angular vector to the object. This can be extracted through a triangulation process. If there are multiple objects within the detection range, their resulting sinusoidal components will be additive with each other. Therefore, the output of the RF front end will be a waveform for which the frequency spectrum will contain components representing the distance and velocity of all detectable objects.

To extract the frequency encoded information from the RF front end output, a correlation process or more specifically a Fourier transform is generally used. In the age of digital computing, this can be done fairly efficiently with a digital processor. As shown in figure 2.1, the output of the RF front end is digitized by an ADC, and then the information is extracted through a digital algorithm within the processor.

2.4 Mathematical Theory of FMCW

Throughout this section, the mathematics and operational theory of an FMCW RADAR system will be derived. The structure of the system will follow the structure illustrated in figure 2.1. The major focus on the theory will be targeted towards the overall system, however an understanding of how the theory relates to each individual block will first be important.

2.4.1 The RF Front End

To measure an objects relative distance and velocity, the system will need the capability to transmit a signal, and measure the time it takes to reach the target and reflect back. We know that if we transmit a radio wave, it will travel at the speed of light given the medium of which it is propagating through. For measuring typical distances here on Earth,

if one considers the speed of light in a vacuum is 299,792,458 m/s, it is very difficult to directly measure the time delay. Rather than measuring the time delay directly, a FMCW RADAR system continuously changes the frequency it transmits, and then compares the transmitted frequency with a received frequency to compute and computes the difference. Figure 2.2 illustrates the RF components which make up an FMCW RADAR. The RF components illustrated are listed below.

- A transmitting and receiving antenna
- A LNA (low noise amplifier) for amplifying the received signal
- A PA (power amplifier) for boosting the transmission power
- A VCO (voltage controlled oscillator) for generating the FM signal
- A mixer to perform a multiplication function

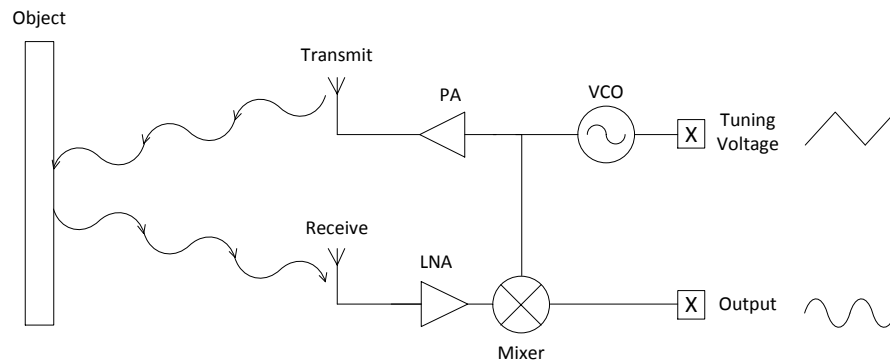


Figure 2.2: FMCW RF Front End System Diagram

Baseband Input and VCO

The RF front end consists of a single baseband input. The input to this block is the VCO tuning voltage as shown in the top right of figure 2.2. The VCO output is described by equation 2.10. As shown in equation 2.10, the output frequency can be changed or

modulated with the input function $V_{tune}(t)$. This result will produce an FM signal, as the FMCW equation in 2.10 is of the same form as the FM equation in 2.9:

$$f_{vco}(t) = A_o \sin \left(2\pi f_c t + K_{vco} \int_{-\infty}^t V_{tune}(\tau) d\tau \right) \quad (2.10)$$

where f_c is the center frequency, A_o is the output amplitude, K_{vco} is the tuning gain, and $V_{tune}(t)$ is the tuning voltage.

For an FMCW application, the tuning voltage (or modulation waveform) will generally consist of baseband function dictating the rate of which frequency should be changed. This waveform may take on any function, however it should be carefully selected such that the desired information can be extracted as easily as possible.

PA and Transmit Antenna

The PA and transmit antenna are the last components making up a transmitter. The VCO output acts as the information source, and requires conditioning before it can be transmitted as an electro-magnetic waveform. The PA is generally uses the greatest amount of power, so high efficiency designs become important. In FM systems (such as FMCW), class C amplifier designs are often used in practice since they can obtain efficiencies as high as 70 % when compared to 25 % efficiency of a class A architecture [10, p.8].

Receive Antenna and LNA

The receive antenna and LNA form the first stages of the receiver. The receive antenna is tuned to be sensitive to EM radiation at the specified system frequencies of operation. Due to this tuning, the antenna will detect the reflected signal energy, and transfer it to the remainder of the receiver.

The LNA is the next component in the signal chain. It is responsible for providing amplification of the received signal. The LNA is expected to have a very high SNR, since the received signal is generally very weak. The higher this ratio, the more sensitive the receiver is, and the better the measurement system will become.

Mixer and Baseband Output

The RF front end has a single baseband output. This output is produced by a heterodyning process, in which the transmitted signal is combined with the received signal to produce

a beat frequency or a frequency difference. The mathematical operation performed by the mixer in an FMCW system produces the baseband output signal. This can be represented as a multiplication of two sinusoids followed by a low-pass filter. The result will be a new sinusoid with a frequency of the difference between the two input frequencies. An example of the pre-filtered mixer output product is given by $f_{heterodyne}(t)$ and is shown in equation 2.11a. The RF module baseband output is then obtained by low-pass filtering the product output to produce $f_{baseband-out}(t)$, which is shown in equation 2.11b. Note that $h_{lpf}(t)$ represents the transfer function of a low-pass filter with adequate bandwidth to only remove the higher frequency component of the heterodyning process, and is convoluted with the product.

$$f_{heterodyne}(t) = \sin(\omega_{tx} t) \cdot \sin(\omega_{rx} t) = \frac{1}{2} [\cos((\omega_{tx} - \omega_{rx}) t) - \cos((\omega_{tx} + \omega_{rx}) t)] \quad (2.11a)$$

$$f_{baseband-out}(t) = f_{heterodyne}(t) \otimes h_{lpf}(t) \approx \frac{1}{2} \cos((\omega_{tx} - \omega_{rx}) t) \quad (2.11b)$$

2.4.2 Combined System Theory

Regardless of the VCO modulation scheme used, the theory remains the same. Two conditions are examined and the mathematical theory is derived in attempt to model the baseband output signal. The first condition examined relates to a single object where both the RADAR and the object remain fixed in distance relative to each other. The second condition examines the condition where the distance between the RADAR and the object is changing at a constant rate due to a relative velocity.

Single Stationary Object

By combining the components described in section 2.4.1, the objective is to measure the delay between transmitting a signal until it is echoed back. The time delay required for the signal to echo is represented as Δt . After determining Δt , the relative distance can then be determined using equation 2.4a. Given any VCO modulation function ($V_{tune}(t)$), the transmitted signal is calculated by equation 2.12a, the received echo is given by equation 2.12b, the heterodyning or mixing output is given by equation 2.12c, and finally the

baseband output is given by equation 2.12d.

$$f_{tx}(t) = A_o \sin \left(2\pi f_c t + K_{vco} \int_{-\infty}^t V_{tune}(\tau) d\tau \right) \quad (2.12a)$$

$$f_{rx}(t) = \frac{B_o}{A_o} f_{tx}(t - \Delta t) = B_o \sin \left(2\pi f_c (t - \Delta t) + K_{vco} \int_{-\infty}^{t-\Delta t} V_{tune}(\tau) d\tau \right) \quad (2.12b)$$

$$\begin{aligned} f_{heterodyne}(t) &= f_{tx}(t) \cdot f_{rx}(t) \\ &= A_o B_o \sin \left(2\pi f_c t + K_{vco} \int_{-\infty}^t V_{tune}(\tau) d\tau \right) \times \dots \\ &\quad \sin \left(2\pi f_c (t - \Delta t) + K_{vco} \int_{-\infty}^{t-\Delta t} V_{tune}(\tau) d\tau \right) \\ &= \frac{A_o B_o}{2} \left\{ \cos \left[2\pi f_c \Delta t + K_{vco} \left(\int_{-\infty}^t V_{tune}(\tau) d\tau - \int_{-\infty}^{t-\Delta t} V_{tune}(\tau) d\tau \right) \right] - \dots \right. \\ &\quad \left. \cos \left[2\pi f_c (2t - \Delta t) + K_{vco} \left(\int_{-\infty}^t V_{tune}(\tau) d\tau + \int_{-\infty}^{t-\Delta t} V_{tune}(\tau) d\tau \right) \right] \right\} \\ &= \frac{A_o B_o}{2} \left\{ \cos \left[2\pi f_c \Delta t + K_{vco} \int_{t-\Delta t}^t V_{tune}(\tau) d\tau \right] - \dots \right. \\ &\quad \left. \cos \left[2\pi f_c (2t - \Delta t) + K_{vco} \left(\int_{-\infty}^t V_{tune}(\tau) d\tau + \int_{-\infty}^{t-\Delta t} V_{tune}(\tau) d\tau \right) \right] \right\} \end{aligned} \quad (2.12c)$$

$$\begin{aligned} f_{baseband-out}(t) &= f_{heterodyne}(t) \otimes h_{lpf}(t) \\ &\approx \boxed{\frac{A_o B_o}{2} \cos \left[2\pi f_c \Delta t + K_{vco} \int_{t-\Delta t}^t V_{tune}(\tau) d\tau \right]} \end{aligned} \quad (2.12d)$$

Equation 2.12a comes from the VCO output as described in equation 2.10. Equation 2.12b is based on the received signal which is a delayed version of the transmitted signal (due to propagation and reflection delays). Equation 2.12c is derived from the heterodyne or mixer functionality which is given in equation 2.11a. Finally, the baseband output in equation 2.12d is derived from the low pass filtering property as shown in equation 2.11b in which the high frequency components are removed.

Single Object with Constant Velocity

To model the impact on the baseband output signal due to a moving object, the same theory presented above will serve as a basis. The transmitted signal $f_{tx}(t)$ will remain the same as shown in 2.13a.

When the object and RADAR have a constant relative velocity between them, the received signal will not only be time-delayed due to the propagation and reflection delay, but it will also experience the [Doppler](#) effect. As shown in equation 2.4b, the received signal's frequency will be increased or decreased by a quantity defined by $f_{doppler}$. Another important property of this effect, is the Fourier transform of the Doppler shifted signal is a [Hermitian](#) function. This implies that the signal remains a real signal, and means the information in the frequency domain remains symmetric around DC.

The exact same procedure described with equations 2.12a through 2.12d may be used. The only difference is the received signal must be frequency shifted to account for the Doppler effect. The frequency shift may be injected by setting $(t - \Delta t) = (t - \Delta t) \cdot (1 + f_{dfactor})$ on the received signal. This is first shown in equation 2.13b.

$$f_{tx}(t) = A_o \sin \left(2\pi f_c t + K_{vco} \int_{-\infty}^t V_{tune}(\tau) d\tau \right) \quad (2.13a)$$

$$\begin{aligned} f_{rx}(t) &= \frac{B_o}{A_o} f_{tx} \left((t - \Delta t) \cdot (1 + f_{dfactor}) \right) \\ &= B_o \sin \left(2\pi f_c (t - \Delta t) \cdot (1 + f_{dfactor}) + K_{vco} \int_{-\infty}^{(t - \Delta t) \cdot (1 + f_{dfactor})} V_{tune}(\tau) d\tau \right) \end{aligned} \quad (2.13b)$$

The multiplication between the two sinusoid signals can be expressed by using the trig identity: $\sin(\alpha) \times \sin(\beta) = \frac{1}{2} [\cos(\alpha - \beta) - \cos(\alpha + \beta)]$. This application is shown in equation 2.13c below. By applying the identity, some simplifications for each angle sum or difference can be performed.

$$\begin{aligned}
f_{heterodyne}(t) &= f_{tx}(t) \cdot f_{rx}(t) \\
&= A_o B_o \sin \left(2\pi f_c t + K_{vco} \int_{-\infty}^t V_{tune}(\tau) d\tau \right) \times \dots \\
&\quad \sin \left(2\pi f_c (t - \Delta t) \cdot (1 + f_{dfactor}) + K_{vco} \int_{-\infty}^{(t-\Delta t) \cdot (1+f_{dfactor})} V_{tune}(\tau) d\tau \right) \\
&= \frac{A_o B_o}{2} \left\{ \cos \left[2\pi f_c \left(\Delta t + (\Delta t - t) \cdot f_{dfactor} \right) + \dots \right. \right. \\
&\quad \left. \left. K_{vco} \left(\int_{-\infty}^t V_{tune}(\tau) d\tau - \int_{-\infty}^{(t-\Delta t) \cdot (1+f_{dfactor})} V_{tune}(\tau) d\tau \right) \right] - \dots \right. \\
&\quad \left. \cos \left[2\pi f_c \left((2 + f_{dfactor}) \cdot t - (1 + f_{dfactor}) \cdot \Delta t \right) + \dots \right. \right. \\
&\quad \left. \left. K_{vco} \left(\int_{-\infty}^t V_{tune}(\tau) d\tau + \int_{-\infty}^{(t-\Delta t) \cdot (1+f_{dfactor})} V_{tune}(\tau) d\tau \right) \right] \right\} \\
&= \frac{A_o B_o}{2} \left\{ \cos \left[2\pi f_c \left(\Delta t + (\Delta t - t) \cdot f_{dfactor} \right) + K_{vco} \int_{(t-\Delta t) \cdot (1+f_{dfactor})}^t V_{tune}(\tau) d\tau \right] - \dots \right. \\
&\quad \left. \cos \left[2\pi f_c \left((2 + f_{dfactor}) \cdot t - (1 + f_{dfactor}) \cdot \Delta t \right) + \dots \right. \right. \\
&\quad \left. \left. K_{vco} \left(\int_{-\infty}^t V_{tune}(\tau) d\tau + \int_{-\infty}^{(t-\Delta t) \cdot (1+f_{dfactor})} V_{tune}(\tau) d\tau \right) \right] \right\}
\end{aligned} \tag{2.13c}$$

The final step in the baseband signal computation is to apply a filter to eliminate the upper sideband. This is done by convolving the heterodyne output with a filter function. An assumption can be made such that a filter with bandwidth such that only the first cosine term will pass through. In an ideal case, the output will exclude the cosine containing the angle sum and the baseband output will consist of only the angle difference. This is shown in equation 2.13d below.

$$\begin{aligned}
f_{baseband-out}(t) &= f_{heterodyne}(t) \otimes h_{lpf}(t) \\
&\approx \boxed{\frac{A_o B_o}{2} \cos \left[2\pi f_c \left(\Delta t + (\Delta t - t) \cdot f_{dfactor} \right) + K_{vco} \int_{(t-\Delta t) \cdot (1+f_{dfactor})}^t V_{tune}(\tau) d\tau \right]}
\end{aligned} \tag{2.13d}$$

The final result of the analysis is shown in equation 2.13d. This analysis is a general solution for any FMCW system's baseband output given propagation delay and Doppler

effects. This equation may be used for both stationary objects, and moving objects. For stationary objects, $f_{dfactor} = 0$, and equation 2.13d becomes identical to equation 2.12d derived for a stationary object. The application of this equation will be shown in section 2.5, and verification through experimentation and field measurements will be shown in chapter 5.

2.5 The FMCW Modulating Waveform

To obtain the desired information based on the system requirements, a few different modulation techniques may be used to generate the transmitted signal. The purpose of the modulation signal is to make use of the architecture and encode a time-stamp or marker which can be used for synchronization. A FMCW RADAR system employs a form of phase or frequency modulation where the information to transmit is contained within the phase or frequency of a carrier wave. A FMCW system uses a direct form to produce this waveform which is described in section 2.4.1. The resulting transmitted waveform is generalized by equation 2.10.

Three common modulation schemes described and analyzed in [11, ch.2]. The modulation scheme is created by generating different modulating waveforms, or different information sources. The three common signals described are: Sawtooth Modulation, Triangular Modulation, and Sinusoidal Modulation. The following three sections will examine each of the common waveforms and describe each one in more detail.

2.5.1 Sawtooth Modulation

Sawtooth modulation is one of the simplest forms of FMCW linear modulation. In this scheme, the VCO frequency is swept in a linearly increasing fashion, producing a linear increase in the frequency of the transmitted signal. This increase in frequency is known as an **up-chirp**. The transmitted signal is piecewise continuous, as it will wrap back to the low frequency once the upper frequency is reached. A derivation of the transmitted signal may be achieved by using the prototype function of equation 2.10, and making the substitutions provided in equations 2.14a to 2.14c. After substituting and solving, the solution representing the transmitted signal is presented in equation 2.14d:

$$K_{vco} = 2\pi f_{tune}\Delta f \tag{2.14a}$$

$$T = \frac{1}{f_{tune}} \quad (2.14b)$$

$$V_{tune}(t) = \left(t - \frac{1}{2f_{tune}} \right) \rightarrow 0 \leq t \leq T \quad (2.14c)$$

$$f_{tx}(t) = A_o \sin \left(2\pi \left[f_c - \frac{\Delta f}{2} \right] t + \frac{2\pi f_{tune} \Delta f}{2} t^2 \right) \quad (2.14d)$$

where A_o is the output amplitude, f_c is the center frequency, Δf is the VCO bandwidth, f_{tune} is the tuning frequency, and t is the time within range of $0 \leq t < \frac{1}{f_{tune}}$.

For a graphical representation, figure 2.3 illustrates a summary of the waveforms associated with producing this modulation scheme.

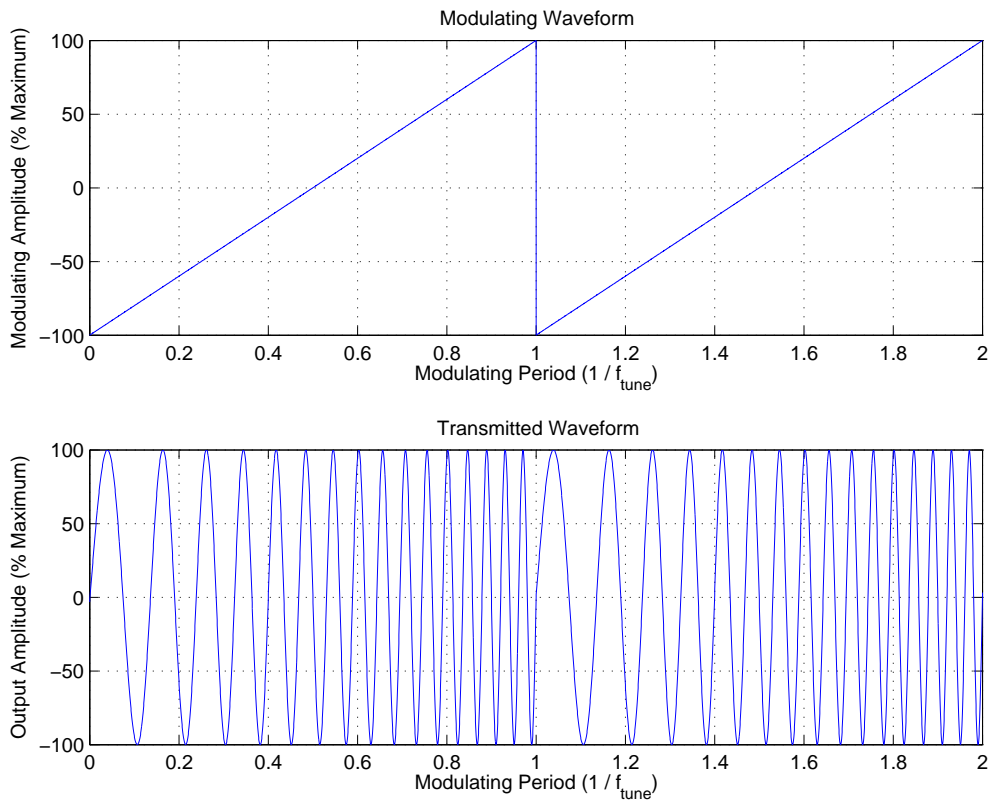


Figure 2.3: Sawtooth Modulation Waveform Overview

To better understand how this modulation scheme can be used for measurements, the combined system theory model outlined in section 2.4.2, specifically the equation derived and shown in 2.13d may be applied. The first step in using the model is to solve the equation shown in 2.15a. This requires replacing the modulating waveform expressions defined in equations 2.14a through 2.14d as shown below.

$$\theta = K_{vco} \int_{(t-\Delta t) \cdot (1+f_{dfactor})}^t V_{tune}(\tau) d\tau \quad (2.15a)$$

$$\theta = 2\pi f_{tune} \Delta f \int_{(t-\Delta t) \cdot (1+f_{dfactor})}^t \left(\tau - \frac{1}{2f_{tune}} \right) d\tau \quad (2.15b)$$

$$\theta = 2\pi f_{tune} \Delta f \left[\frac{\tau^2}{2} - \frac{\tau}{2f_{tune}} \right]_{(t-\Delta t) \cdot (1+f_{dfactor})}^t \quad (2.15c)$$

$$\begin{aligned} \theta &= 2\pi f_{tune} \Delta f \left[\frac{t^2}{2} - \frac{t}{2f_{tune}} - \frac{(t-\Delta t)^2 \cdot (1+f_{dfactor})^2}{2} + \frac{(t-\Delta t) \cdot (1+f_{dfactor})}{2f_{tune}} \right] \\ &= 2\pi f_{tune} \Delta f \left[\frac{t^2}{2} - \frac{t}{2f_{tune}} - \frac{(t^2 - 2t\Delta t + \Delta t^2) \cdot (1+2f_{dfactor} + f_{dfactor}^2)}{2} + \frac{t - \Delta t + f_{dfactor}t - f_{dfactor}\Delta t}{2f_{tune}} \right] \\ &= 2\pi f_{tune} \Delta f \left[\frac{t^2 - t^2 + 2t\Delta t - \Delta t^2}{2} - \frac{(t^2 - 2t\Delta t + \Delta t^2) \cdot (2f_{dfactor} + f_{dfactor}^2)}{2} + \frac{f_{dfactor}t - f_{dfactor}\Delta t - \Delta t}{2f_{tune}} \right] \\ &= 2\pi f_{tune} \Delta f \left[\frac{2t\Delta t - \Delta t^2}{2} - \frac{(t^2 - 2t\Delta t + \Delta t^2) \cdot (2f_{dfactor} + f_{dfactor}^2)}{2} + \frac{f_{dfactor}t - f_{dfactor}\Delta t - \Delta t}{2f_{tune}} \right] \end{aligned} \quad (2.15d)$$

At this point, some assumptions to simplify the calculations may be made. Looking back on the definition of $f_{dfactor}$ (equation 2.4c), if we assume $c \gg \Delta V$, then we can assume $f_{dfactor}^2 \approx 0$. This assumption means we will only be measuring objects with a velocity much less than the speed of light.

Secondly, if we look at the relationship between Δt and Δd (equation 2.4a), we can assume $c \gg \Delta d$. With this assumption, we can also assume that $\Delta t^2 \approx 0$. This means that we will only be measuring objects in close range that result in a small reflection delay.

$$\begin{aligned}
\theta &= 2\pi f_{tune} \Delta f \left[\frac{2t\Delta t}{2} - \frac{(t^2 - 2t\Delta t) \cdot (2f_{dfactor})}{2} + \frac{f_{dfactor}t - f_{dfactor}\Delta t - \Delta t}{2f_{tune}} \right] \\
&= 2\pi f_{tune} \Delta f \left[\frac{t \cdot (2\Delta t + 4f_{dfactor}\Delta t + \frac{f_{dfactor}}{f_{tune}})}{2} - \frac{\Delta t(1 + f_{dfactor})}{2f_{tune}} - t^2 \cdot f_{dfactor} \right]
\end{aligned} \tag{2.15e}$$

To compute the baseband output using the calculation derived in 2.15e, it must be plugged into the model provided by equation 2.13d. This is provided in equation 2.16a for a moving object, and simplified in equation 2.16b for a stationary object. As a final note, these equations are only valid in the range of $0 \leq t < \frac{1}{f_{tune}}$ as defined in equation 2.14d above.

$$\begin{aligned}
f_{baseband-out} &= \frac{A_o B_o}{2} \cos \left[2\pi f_c \left(\Delta t + (\Delta t - t) \cdot f_{dfactor} \right) + \dots \right. \\
&\quad \left. 2\pi f_{tune} \Delta f \left[\frac{t \cdot (2\Delta t + 4f_{dfactor}\Delta t + \frac{f_{dfactor}}{f_{tune}})}{2} - \frac{\Delta t(1 + f_{dfactor})}{2f_{tune}} - t^2 \cdot f_{dfactor} \right] \right]
\end{aligned} \tag{2.16a}$$

$$f_{baseband-out} = \frac{A_o B_o}{2} \cos \left[2\pi f_c \Delta t + 2\pi f_{tune} \Delta f \left[t\Delta t - \frac{\Delta t}{2f_{tune}} \right] \right] \tag{2.16b}$$

To perform a measurement using a Sawtooth Modulation scheme, the RF front end described in section 2.4.1 will perform a frequency difference calculation, by producing a tone with a frequency equal to the difference between the transmitted and received frequency. The baseband output is given in equations 2.16a (moving object), and 2.16b (stationary object).

Figure 2.4 illustrates the transmitted frequency and received frequency. In the example illustrated in the figure, it should be noted that the time delay required for the signal to reach the target and reflect back will shift the dotted RX trace to the right. The further the object, the longer the propagation delay, and the further right the RX trace is shifted. It must also be noted that if the objects are moving, the RX trace will be subjected to a Doppler shift. The effect will be the trace will be shifted up or down depending on the direction of motion. It can be seen in the illustration that this creates ambiguity in the frequency difference, as the Doppler shift increases the frequency just as the propagation delay does.

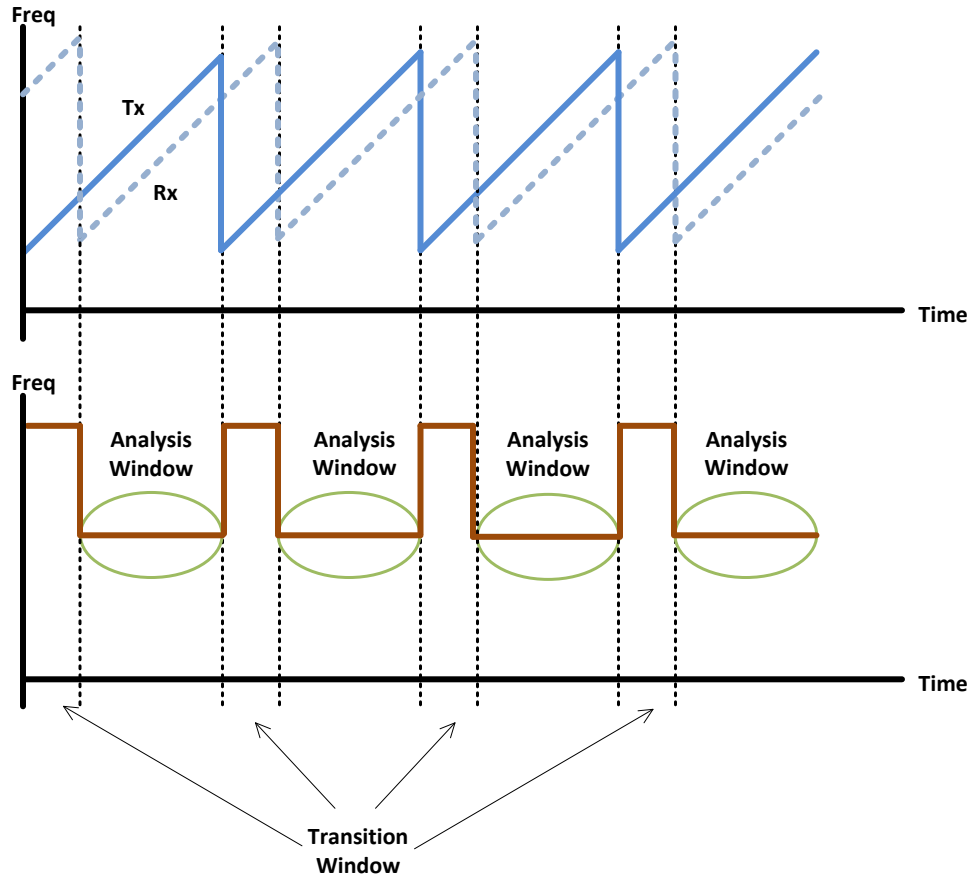


Figure 2.4: Sawtooth Modulation Frequency Difference

As a simplification of equation 2.16a, the baseband frequency in the analysis window can be estimated graphically using figure 2.4, as done in many textbooks. The rate that the transmit frequency changes is $\Delta f \times f_{tune}$ Hz/sec.

First assuming a stationary object, after Δt seconds, the transmit frequency will have increased by $\Delta f \times f_{tune} \times \Delta t$ Hz. This means the expected baseband output should be at this frequency. Comparing with equation 2.16b shows the model output produces a frequency of $\Delta f \times f_{tune} \times \Delta t$ Hz. This is visualized by a right shift by Δt seconds of the received frequency when compared to the transmit frequency in figure 2.4. The baseband output is the frequency difference between the transmitted and received signal, and is

constant in the illustrated analysis window.

Next assuming a moving object, there will be an additional difference component due to the [Doppler](#) shift. This Doppler shift is generally approximated as $f_c \times f_{dfactor}$ for narrow-band systems, where the assumption is the Doppler shift is exactly the same throughout the entire transmitted frequency range. This additional component is represented in the model as shown in equation [2.16a](#). Graphically, this represents a shift in the received frequency relative to the transmitted frequency, and can not be distinguished between a propagation delay.

Because of the inability of this system to distinguish between a frequency difference caused by a propagation delay and a [Doppler](#) shift, this system can not measure both distance and velocity unless further baseband processing is performed (i.e., results taken over many measurement periods are compared with each other).

2.5.2 Triangular Modulation

The triangular wave modulation scheme appears to be the most widely used scheme in the literature reviewed. By using a triangular waveform to modulate the FM carrier, it is possible to obtain both distance and velocity information. To consider triangular modulation, it is necessary to break the modulation into two separate sections (an up-chirp, and a down-chirp), since the modulating waveform is periodic but not continuous. A derivation of the transmitted signal may be achieved by using the prototype function of equation [2.10](#), and making the substitutions provided in equations [2.17a](#) to [2.17c](#). After substituting and solving, the final solution is presented in equation [2.17d](#):

$$K_{vco} = 2\pi f_{tune} \Delta f \tag{2.17a}$$

$$T = \frac{1}{f_{tune}} \tag{2.17b}$$

$$V_{tune}(t) = \begin{cases} \left(2t - \frac{1}{2f_{tune}}\right) & : 0 \leq t < \frac{T}{2} \\ \left(\frac{3}{2f_{tune}} - 2t\right) & : \frac{T}{2} \leq t < T \end{cases} \tag{2.17c}$$

$$f_{tx}(t) = \begin{cases} A_o \sin \left(2\pi \left[f_c - \frac{\Delta f}{2} \right] t + 2\pi f_{tune} \Delta f \cdot t^2 \right) & : 0 \leq t < \frac{1}{2f_{tune}} \\ A_o \sin \left(2\pi \left[f_c + \frac{3\Delta f}{2} \right] t - 2\pi f_{tune} \Delta f \cdot t^2 \right) & : \frac{1}{2f_{tune}} \leq t < \frac{1}{f_{tune}} \end{cases} \quad (2.17d)$$

where A_o is the output amplitude, f_c is the center frequency, Δf is the VCO bandwidth, f_{tune} is the tuning frequency, and t represents time in the appropriately defined intervals.

For a graphical representation, figure 2.5 illustrates a summary of the waveforms associated with producing this modulation scheme.

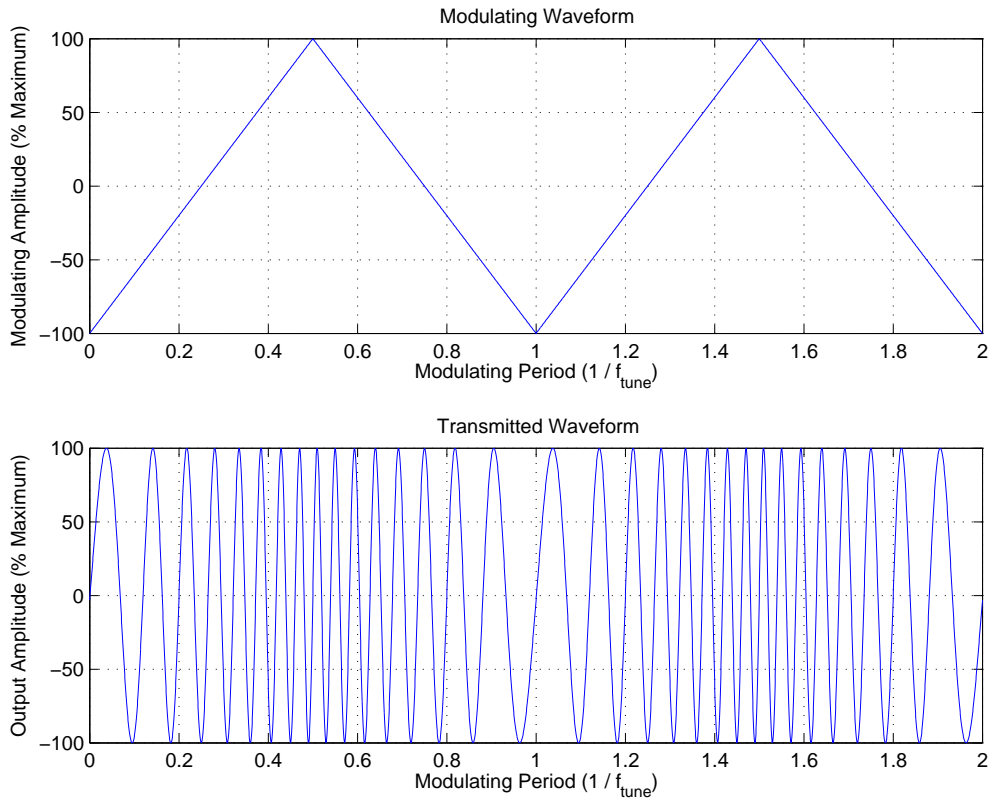


Figure 2.5: Triangle Modulation Waveforms

The calculation of the baseband output is nearly identical to that in section 2.5.1, however two equations must be derived where one is for the up-chirp, and one is for the

down-chirp. The derivation for the up-chirp will be done first, and is shown in equations 2.18a through 2.18e.

$$\theta_{up-chirp} = K_{vco} \int_{(t-\Delta t) \cdot (1+f_{dfactor})}^t V_{tune-up}(\tau) d\tau \quad (2.18a)$$

$$\theta_{up-chirp} = 2\pi f_{tune} \Delta f \int_{(t-\Delta t) \cdot (1+f_{dfactor})}^t \left(2\tau - \frac{1}{2f_{tune}} \right) d\tau \quad (2.18b)$$

$$\theta_{up-chirp} = 2\pi f_{tune} \Delta f \left[\tau^2 - \frac{\tau}{2f_{tune}} \right]_{(t-\Delta t) \cdot (1+f_{dfactor})}^t \quad (2.18c)$$

$$\theta_{up-chirp} = 2\pi f_{tune} \Delta f \left[t^2 - \frac{t}{2f_{tune}} - (t - \Delta t)^2 \cdot (1 + f_{dfactor})^2 + \frac{(t-\Delta t) \cdot (1+f_{dfactor})}{2f_{tune}} \right] \quad (2.18d)$$

At this point, we can make the same assumptions to simplify the calculations. Looking back on the definition of $f_{dfactor}$ (equation 2.4c), if we assume $c \gg \Delta V$, then we can assume $f_{dfactor}^2 \approx 0$. This assumption means we will only be measuring objects with a velocity much less than the speed of light.

Secondly, if we look at the relationship between Δt and Δd (equation 2.4a), we can assume $c \gg \Delta d$. With this assumption, we can also assume that $\Delta t^2 \approx 0$. This means that we will only be measuring objects in close range that result in a small reflection delay.

$$\begin{aligned} \theta_{up-chirp} &= 2\pi f_{tune} \Delta f \left[t^2 - \frac{t}{2f_{tune}} - (t^2 - 2t\Delta t) \cdot (1 + 2f_{dfactor}) + \frac{(t-\Delta t) \cdot (1+f_{dfactor})}{2f_{tune}} \right] \\ &= 2\pi f_{tune} \Delta f \left[t \cdot (2\Delta t + 4f_{dfactor} \Delta t + \frac{f_{dfactor}}{2f_{tune}}) - \frac{\Delta t(1+f_{dfactor})}{2f_{tune}} - 2t^2 \cdot f_{dfactor} \right] \end{aligned} \quad (2.18e)$$

Using the exact same procedure and approximations, the down-chirp expression is derived and shown in equation 2.19a.

$$\theta_{down-chirp} = 2\pi f_{tune} \Delta f \left[\frac{3\Delta t(1+f_{dfactor})}{2f_{tune}} - t \cdot (2\Delta t + 4f_{dfactor}\Delta t + \frac{3f_{dfactor}}{2f_{tune}}) + 2t^2 \cdot f_{dfactor} \right] \quad (2.19a)$$

To compute the baseband output using the calculations derived in 2.18e and 2.19a, they must be plugged into the model provided by equation 2.13d. This is provided in equations 2.20a and 2.21a for a moving object. The calculation is then simplified in equations 2.20b and 2.21b for a stationary object. As a final note, equations 2.20a and 2.20b are only valid in the range of: $0 \leq t < \frac{1}{2f_{tune}}$. Equations 2.21a and 2.21b are only valid in the range of: $\frac{1}{2f_{tune}} \leq t < \frac{1}{f_{tune}}$.

$$f_{baseband-out} = \frac{A_o B_o}{2} \cos \left[2\pi f_c \left(\Delta t + (\Delta t - t) \cdot f_{dfactor} \right) + \dots \right. \\ \left. 2\pi f_{tune} \Delta f \left[t \cdot \left(2\Delta t + 4f_{dfactor}\Delta t + \frac{f_{dfactor}}{2f_{tune}} \right) - \dots \right. \right. \quad (2.20a) \\ \left. \left. \frac{\Delta t(1+f_{dfactor})}{2f_{tune}} - 2t^2 \cdot f_{dfactor} \right] \right]$$

$$f_{baseband-out} = \frac{A_o B_o}{2} \cos \left[2\pi f_c \Delta t + 2\pi f_{tune} \Delta f \left[2t\Delta t - \frac{\Delta t}{2f_{tune}} \right] \right] \quad (2.20b)$$

$$f_{baseband-out} = \frac{A_o B_o}{2} \cos \left[2\pi f_c \left(\Delta t + (\Delta t - t) \cdot f_{dfactor} \right) + \dots \right. \\ \left. 2\pi f_{tune} \Delta f \left[\frac{3\Delta t(1+f_{dfactor})}{2f_{tune}} + 2t^2 \cdot f_{dfactor} - \dots \right. \right. \quad (2.21a) \\ \left. \left. t \cdot \left(2\Delta t + 4f_{dfactor}\Delta t + \frac{f_{dfactor}}{2f_{tune}} \right) \right] \right]$$

$$f_{baseband-out} = \frac{A_o B_o}{2} \cos \left[2\pi f_c \Delta t + 2\pi f_{tune} \Delta f \left[\frac{3\Delta t}{2f_{tune}} - 2t\Delta t \right] \right] \quad (2.21b)$$

To perform a measurement using a triangular modulation scheme, the RF front end described in section 2.4.1 will perform a frequency difference calculation, by producing

a tone with a frequency equal to the difference between the transmitted and received frequency. Figure 2.6 illustrates the transmitted frequency and received frequency. In the example illustrated, it should be noted that the time delay required for the signal to reach the target and reflect back will shift the RX trace to the right. The further the object, the longer the propagation delay, and the further right the RX trace is shifted. It must also be noted that if the objects are moving, the RX trace will be subjected to a Doppler shift. The effect will be the trace will be shifted up or down depending on the direction of motion. It can be seen in the illustration that this creates ambiguity in the frequency difference, as the Doppler shift creates the same effect as the propagation delay.

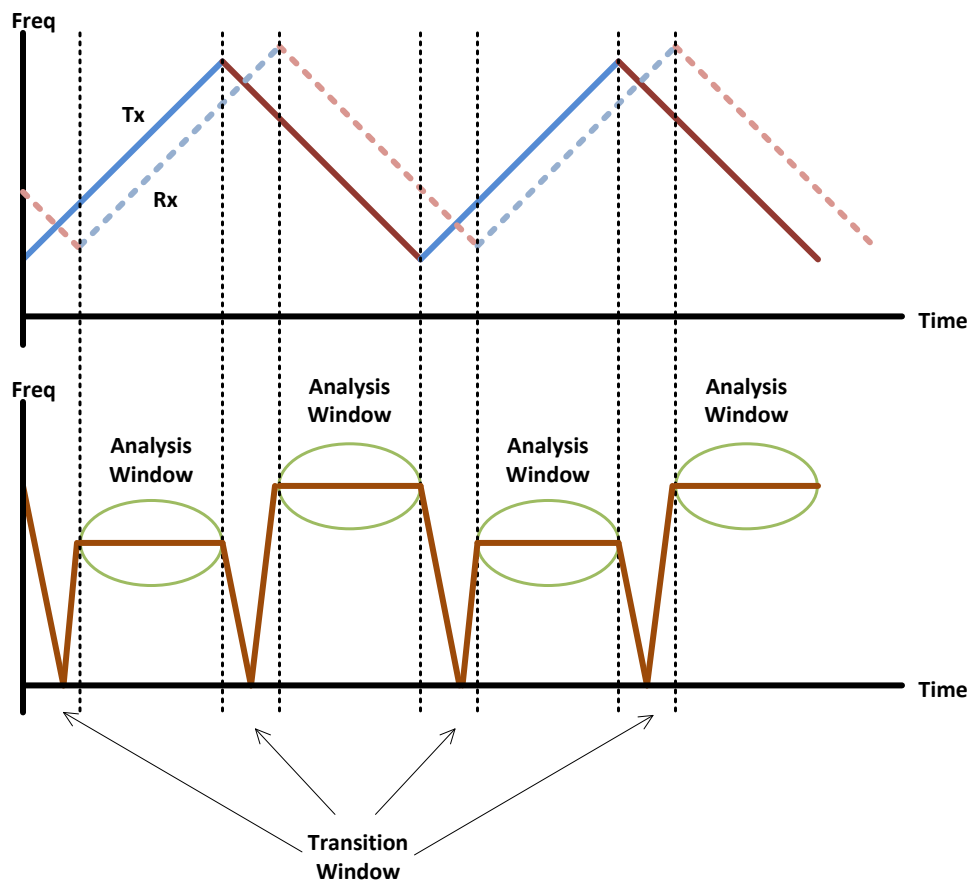


Figure 2.6: Triangular Modulation Frequency Difference

As a simplification of equations 2.20a and 2.21a, the baseband frequency in the analysis window can be estimated graphically using figure 2.6, as done in many textbooks. The rate that the transmit frequency changes is $\Delta f \times 2f_{tune}$ Hz/sec (positive for the up-chirp case, and negative for the down-chirp case).

First assuming a stationary object, after Δt seconds, the transmit frequency will increase by $\Delta f \times 2f_{tune} \times \Delta t$ Hz. This means the expected baseband output should be at this frequency. Comparing with equation 2.20b shows the model output produces a frequency of $\Delta f \times 2f_{tune} \times \Delta t$ Hz. This is visualized by a right shift by Δt seconds of the received frequency when compared to the transmit frequency in figure 2.4. The baseband output is the frequency difference between the transmitted and received signal, and is constant in the illustrated analysis window.

Next assuming a moving object, there will be an additional difference component due to the Doppler shift. This Doppler shift is generally approximated as $f_c \times f_{dfactor}$ for narrow-band systems, where the assumption is the Doppler shift is exactly the same throughout the entire transmitted frequency range. This additional component is represented in the model as shown in equations 2.20a and 2.21a. Graphically, this represents an up/down shift in the received frequency relative to the transmitted frequency. Because the up-chirp and down-chirp have the same magnitude but different sign, the Doppler component can be easily extracted by examining both positive and negative chirps.

By averaging the frequency measured in both up-chirp and down-chirp analysis windows, the Doppler shift will cancel out and the result left over will simply be the propagation delay component. Next, to obtain the Doppler component, the distance between the average and either up/down chirp will provide the contribution due to the Doppler shift.

2.5.3 Sinusoidal Modulation

By using a sinusoid waveform to modulate the FM carrier, it is possible to obtain velocity information. A description of this modulation scheme is provided in [8, p.88]. By using a sinusoid to modulate the FM carrier, it is possible to obtain distance and velocity information. A derivation of the transmitted signal may be achieved by using the prototype function of equation 2.10, and making the substitutions provided in equations 2.22a to 2.22c. After substituting and solving, the solution is presented in equation 2.22d:

$$K_{vco} = \frac{2\pi\Delta f}{2} \tag{2.22a}$$

$$T = \frac{1}{f_{tune}} \quad (2.22b)$$

$$V_{tune}(t) = \cos(2\pi f_{tune}t) \rightarrow 0 \leq t \leq T \quad (2.22c)$$

$$f_{tx}(t) = A_o \sin \left(2\pi f_c t + \frac{\Delta f}{2f_{tune}} \sin(2\pi f_{tune} t) \right) \quad (2.22d)$$

where A_o is the output amplitude, f_c is the center frequency, Δf is the VCO bandwidth, f_{tune} is the tuning frequency, and t is the time within the range $0 \leq t < \frac{1}{f_{tune}}$.

For a graphical representation, figure 2.7 illustrates a summary of the waveforms associated with producing this modulation scheme.

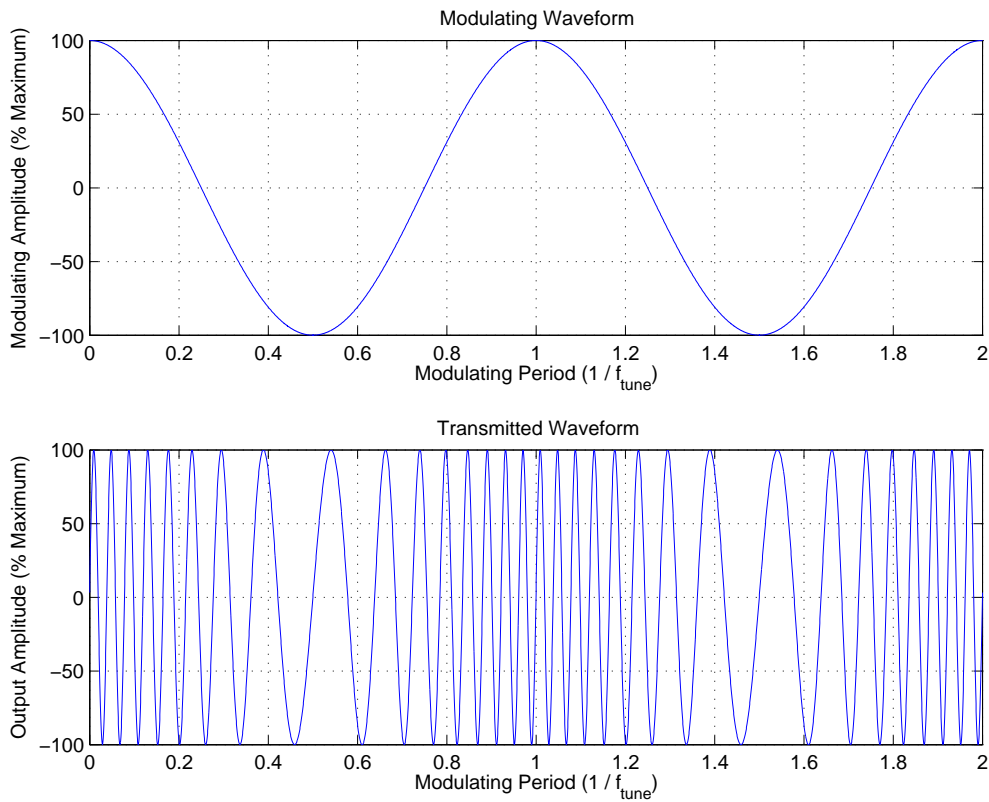


Figure 2.7: Sinusoidal Modulation Waveforms

To better understand how this modulation scheme can be used for measurements, the combined system theory model outlined in section 2.4.2, specifically the equation derived and shown in 2.13d may be applied. The first step in using the model is to solve the equation shown in 2.23a. This requires replacing the modulating waveform expressions defined in equations 2.22a through 2.22d

$$\theta = K_{vco} \int_{(t-\Delta t) \cdot (1+f_{dfactor})}^t V_{tune}(\tau) d\tau \quad (2.23a)$$

$$\theta = \frac{2\pi\Delta f}{2} \int_{(t-\Delta t) \cdot (1+f_{dfactor})}^t \cos(2\pi f_{tune}\tau) d\tau \quad (2.23b)$$

$$\theta = \frac{\Delta f}{2f_{tune}} \left[\sin(2\pi f_{tune} \tau) \right]_{(t-\Delta t) \cdot (1+f_{dfactor})}^t \quad (2.23c)$$

$$\theta = \frac{\Delta f}{2f_{tune}} \left[\sin(2\pi f_{tune} t) - \sin(2\pi f_{tune} (t - \Delta t) \cdot (1 + f_{dfactor})) \right] \quad (2.23d)$$

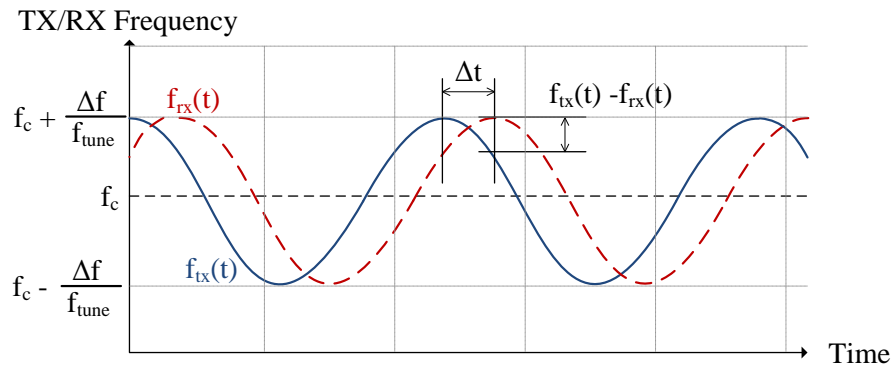
To compute the baseband output using the calculation derived in 2.23d, it must be plugged into the model provided by equation 2.13d. This is provided in equation 2.24a for a moving object, and simplified in equation 2.24b for a stationary object. As a final note, these equations are only valid in the range of: $0 \leq t < \frac{1}{f_{tune}}$ as defined in equation 2.22d above.

$$f_{baseband-out} = \frac{A_o B_o}{2} \cos \left[2\pi f_c \left(\Delta t + (\Delta t - t) \cdot f_{dfactor} \right) + \dots \right. \\ \left. \frac{\Delta f}{2f_{tune}} \left[\sin(2\pi f_{tune} t) - \sin(2\pi f_{tune} (t - \Delta t) \cdot (1 + f_{dfactor})) \right] \right] \quad (2.24a)$$

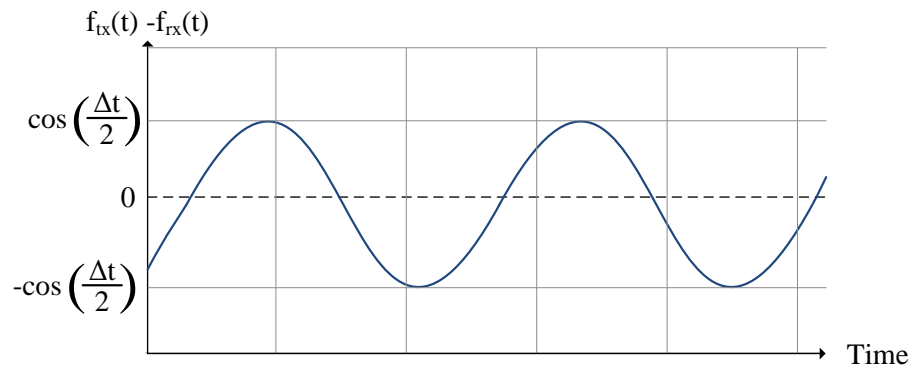
$$f_{baseband-out} = \frac{A_o B_o}{2} \cos \left[2\pi f_c \Delta t + \frac{\Delta f}{f_{tune}} \left[\cos(2\pi f_{tune} \frac{\Delta t}{2}) \times \cos(2\pi f_{tune} t) \right] \right] \quad (2.24b)$$

To perform a measurement using a Sinusoidal modulation scheme, the RF front end described in section 2.4.1 will perform a frequency difference calculation. Unlike the triangular or sawtooth modulation schemes, with a sinusoidal modulation the object's distance and velocity is encoded as a change in angle rather than a constant angle. As shown in equations 2.24a and 2.24b, the baseband output is of similar form to a FM or PM signal.

As the transmitter produces the EM wave, the frequency which is sent into space changes according to equation 2.22d. As the wave propagates towards the target, the frequency does not change unless a Doppler shift occurs. The transmitted frequency (f_{tx}) is shown as the solid blue line in figure 2.8(a), as it changes as a function of time. Due to the propagation time (assuming no Doppler shift), the received frequency will follow the same pattern as the transmitted waveform, and is shown in figure 2.8(a) as the red curve (f_{rx}). Figure 2.8(b) illustrates the baseband sinusoid change in frequency vs time.



(a) TX and RX Frequency vs Time



(b) Baseband Output Frequency vs Time

Figure 2.8: FMCW Sinusoid Modulation Frequency vs Time

Chapter 3

Baseband and Processing Optimization

By taking the final application of the sensor into account, there is a lot of potential to optimize the radar system to reduce cost and complexity. The reason is because absolute precision is not necessarily required for powertrain control sensors, since the results are not used for safety critical decisions. Nevertheless, the data returned by the sensor must meet the minimum requirements of the smart powertrain system such that the fuel efficiency improvements by enabling the algorithm approach the theoretical simulated estimates. The two main considerations used when optimizing are the required RF output signal bandwidth, and the processing requirements needed to extract the information.

The RF output signal bandwidth is significant in the overall cost, because it dictates the constraints on the analog to digital converter (not only in design requirements, but also with respect to power consumption). Since this signal is the analysis signal that contains the desired information, it will have to be converted to the digital domain before any processing can be performed. The advantage to minimizing this bandwidth is to save cost in conversion signal chain required to digitize this signal. Generally an analog to digital converter with a high bandwidth will have a bit resolution or dynamic range that is less than an analog to digital converter with a low bandwidth. This means as the bandwidth of a data converter increases, the dynamic range will decrease. The assumption is for relatively the same cost, a high bandwidth and low resolution data converter can be replaced with a low bandwidth and high resolution data converter. The advantage to making this change is by increasing the dynamic of the data converter, is the possibility to simplify or even eliminate complex high-component-count analog filter / dynamic gain front ends. Since the system will want to detect both close and far objects, the front end

will have to allow for detecting large signals (close objects) as well as small signals (far objects). With more dynamic range, the system may be more capable of detecting both signals together without dynamically adjusting any other gains.

Additionally, the computational requirements needed to process the signal are a significant contributor to overall cost, because the algorithm will require enough processing capability to perform the required analysis. To begin analyzing what tradeoffs can be made in the sensor design, it is important to first understand how the detected frequencies in the up-chirp and down-chirp sections are used to determine the objects distance and velocity. The theory and derivation is described in more detail in [5] and [6]. This section also served the basis for the published conference paper [12, p.84 - p.89].

3.1 Introduction to simplifications

As previously described, the functional partitioning can be broken down into four main groups. An RF Front End will receive a tuning voltage input and will transmit a frequency proportional to this voltage. It will also output a signal which will contain encoded information representing an objects distance and velocity. An analog to digital converter is needed to convert this signal into the digital domain, allowing for digital signal processing algorithms to decode and extract the desired information. A processor is required to perform these calculations. In addition, with proper synchronization between the tuning voltage and the processing algorithm, it is possible to make some simplifications in the fully derived model in section 2.2.

To obtain both distance and velocity information of an object most efficiently, a triangular modulation scheme is employed as described in section 2.5.2. With this modulation scheme, the VCO tuning voltage will increase (up-chirp) and then decrease (down-chirp) in a linear ramp fashion. This will allow measurement of both delay (range), Doppler shift (velocity). The frequency detector must be synchronous with the VCO tuning voltage in order to analyze the output individually and efficiently. Figure 3.1 illustrates this concept. The upper plot represents the transmitted / received frequency versus time, and the lower plot represents the FMCW radar front end frequency output.

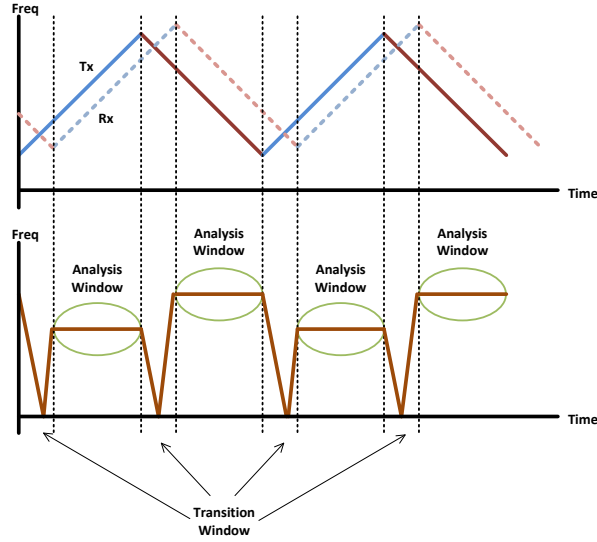


Figure 3.1: FMCW Triangle Modulation Output Frequency vs Time

Notice that if the analysis is performed only in the analysis window, the theory and equations from Chapter 2.2 can be simplified as the analysis will only consist of a single sinusoid with frequency proportional to the difference between transmitted and received signals. These expressions are commonly used expressions found and derived in most literature, and may be found in [8, p.82].

$$f_{range} = \frac{2\Delta d\Delta f}{Tc} \quad (3.1a)$$

where Δd is the object distance, Δf is the VCO tuning bandwidth, T is the time to sweep from max to min frequency, and c is the speed of light.

The second part of the frequency difference which must be accounted for is the component introduced by the Doppler effect. This effect will introduce a frequency shift when there is a relative velocity between the sensor and the object being detected. The frequency component introduced is given by equation 3.1b:

$$f_{doppler} = \frac{2\Delta v f_{avg}}{c} \quad (3.1b)$$

where Δv is the object velocity, f_{avg} is the average frequency given by $\frac{f_{VCO-max} - f_{VCO-min}}{2}$, and c is the speed of light.

The frequency expected to be observed within the up-chirp and down-chirp analysis windows is given by the following two expressions in equations 3.1c and 3.1d.

$$f_{up-chirp} = f_{range} - f_{doppler} \quad (3.1c)$$

$$f_{down-chirp} = f_{range} + f_{doppler} \quad (3.1d)$$

By combining the analysis measurements described in equations 3.1c and 3.1d, it is possible to obtain an expression for both the range and Doppler components. The results are described in equations 3.1e and 3.1f.

$$f_{range} = \frac{f_{up-chirp} + f_{down-chirp}}{2} \quad (3.1e)$$

$$f_{doppler} = \frac{f_{down-chirp} - f_{up-chirp}}{2} \quad (3.1f)$$

Finally, as shown in equations 3.1g and 3.1h, it is possible to calculate both object distance and velocity.

$$\Delta d = \frac{(f_{up-chirp} + f_{down-chirp}) T c}{4 \Delta f} \quad (3.1g)$$

$$\Delta v = \frac{(f_{down-chirp} - f_{up-chirp}) c}{4 f_{avg}} \quad (3.1h)$$

By performing a up-chirp and down-chirp measurement, it will require a time duration of T seconds. By performing these two measurements, it is then theoretically possible to obtain a measurement of both distance and velocity.

3.2 Combining Theory with Signal Processing

As described above and apparent in equations 3.1c and 3.1d, the maximum range and velocity required will play a part in determining the bandwidth required for analysis. In

addition, equation 3.1f shows that the only parameter which can tweak the relationship between the Doppler component and the relative velocity is f_{avg} . This means that given the selected RF bandwidth to be used, the Doppler shift contribution will be fixed based on the specifications. Finally, equation 3.1a shows that the frequency contribution is inversely proportional to T (i.e., rate that the VCO is modulated). This final point provides the basis for tuning. As an example of how the system may be tuned, the following table summarizes the initial specifications of the system.

Table 3.1: System Specifications

Parameter	Value	Units
Minimum RF VCO Frequency	24.000	GHz
Maximum RF VCO Frequency	24.250	GHz
Maximum Object Distance	250	m
Maximum Object Velocity (not relative)	150	km/h

Note that the 24 GHz band was selected as it is currently allocated as an industrial, scientific and medical (ISM) band and has a technology cost lower than 77 GHz radar technology. As such, it is currently a commonly used band for automotive radar.

When considering the analysis is performed using a digital DFT (discrete Fourier transform), the algorithm can be optimized into a radix-2 form when the number of points (N) is an integer power of two. We also know that the analysis has to be done during the full up-chirp and the full down-chirp, which has a time defined by T. To satisfy the Nyquist sample theorem, the ADC sample frequency (F_s) must be 2x the maximum signal frequency (f_{max}). This allows new constraints as defined in equations 3.2a and 3.2b.

$$N = F_s T \tag{3.2a}$$

$$F_s = 2f_{max} \tag{3.2b}$$

The next step is to determine the maximum bandwidth of the RF front end which will need to be analyzed (f_{max}). By reducing this bandwidth, significant constraints are

reduced on the data converter and on the signal processing, hence reducing the cost of the system. The maximum analysis bandwidth required is calculated when both equations 3.1a and 3.1b are maximum as shown in equation 3.2c.

$$f_{max} = f_{range} (\Delta d = \Delta d_{max}) + f_{doppler} (\Delta v = \Delta v_{max}) \quad (3.2c)$$

Finally, the overall system tuning can be tied together by combining equations 3.1a, 3.1b, 3.2a, 3.2b, and 3.2c. This results in a relationship and constraint shown in equations 3.2d and 3.2e. The constraint comes from requiring a positive denominator.

$$F_s = \frac{4N\Delta v_{max}f_{avg}}{Nc - 4\Delta f\Delta d_{max}} \quad (3.2d)$$

$$N \geq \frac{4\Delta f\Delta d_{max}}{c} \quad (3.2e)$$

It is perhaps difficult to see, but equation 3.2d shows as N increases, (F_s) decreases. This means to have a small analysis bandwidth, you will need to have a large N. In terms of cost, this is a conflicting requirement, because a larger N requires more computational resources to do the analysis. This means the optimization does not have a concrete solution, but rather illustrates the possible tradeoffs between bandwidth and computational requirements.

To select a reasonable value, equation 3.2e sets the starting point. Given the requirements from table 3.1, the minimum N is 834. Taking into account that an integer power of 2 is needed to optimize the DFT algorithm, the following table summarizes the tradeoff between N, F_s , and Processing Cost. The processing cost was evaluated using the analysis conducted in [13] by accumulating the operations required for the radix-2 PM algorithm.

Table 3.2: N vs F_s and Processing Cost tradeoff

N	F_s (ksps)	Processing Cost (Operations)
1024	143.9	46590
2048	45.20	104444
4096	33.65	231418

It can be seen as summarized in Table 3.2, that going from $N=1024$ to $N=2048$ results in almost a 70% reduction of F_s , but going from $N=2048$ to $N=4096$ results in roughly only 25% reduction in F_s . Therefore, it is arguable that using $N=2048$ will result in a reasonable tradeoff between analysis bandwidth and processing requirements. What is not included in this analysis however, are memory requirements, and processor architecture efficiency. It is true that even though the number of processing operations increases with N , the amount of time given to complete them will also increase (making the operations per second decrease). A complete analysis as such is difficult to generalize, because the efficiency will be largely dependent on the processor architecture used to realize the DFT algorithm. For example, a multiplication may take more time to perform than an addition or a move operation. Without detailed knowledge of the architecture, it is difficult use operations per second as a metric. The following illustration shown in figure 3.2 illustrates the tradeoff of N and , showing that for $N=2048$ the most optimal tradeoff can be achieved.

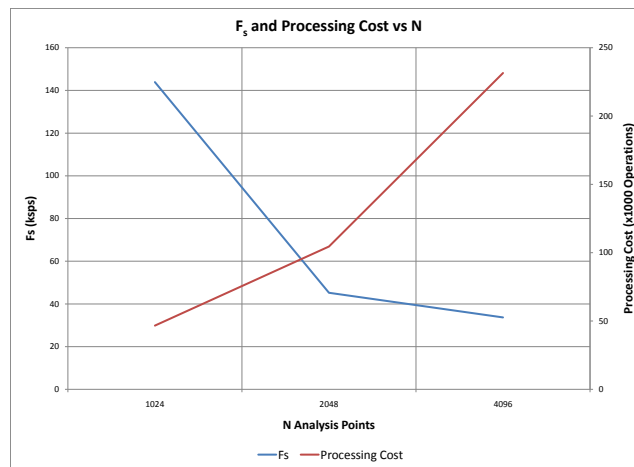


Figure 3.2: F_s and Processing Cost vs N

By selecting $N=2048$, the remaining parameters can be computed. The resulting parameters are summarized in table 3.3 below.

Table 3.3: System Tuned Parameters

Parameter	Value	Units
Δf (VCO bandwidth)	250.00	MHz
T (VCO modulation period)	45.331	ms
f_{avg} (center frequency)	24.125	GHz
c (velocity of EM wave)	3.0000×10^8	m/s
Maximum $f_{doppler}$ (Doppler shift)	13.403	kHz
F_s (ADC Sample Frequency)	45.195	ksps
N (Processing window for each chirp)	2048	samples

Chapter 4

Prototyping Platform and System Realization

4.1 Introduction

Throughout the research conducted as part of this thesis, it has been desired to prove the theory and perform physical measurements to validate the results. To facilitate an easy mechanism for prototyping and field testing, a system consisting of hardware and software was required. To allow for maximum flexibility given the uncertainty of what exactly will be required to prototype the system, a custom design was conceived with this project as well as possible future projects in mind.

For the purposes of this project, it is desirable to have a system capable of verifying the relationship between the baseband frequency, and a physical object distance. A block diagram for this is shown in figure [4.1](#). For the purposes of this project, all the processing and analysis is to be performed on a PC, using MATLAB.

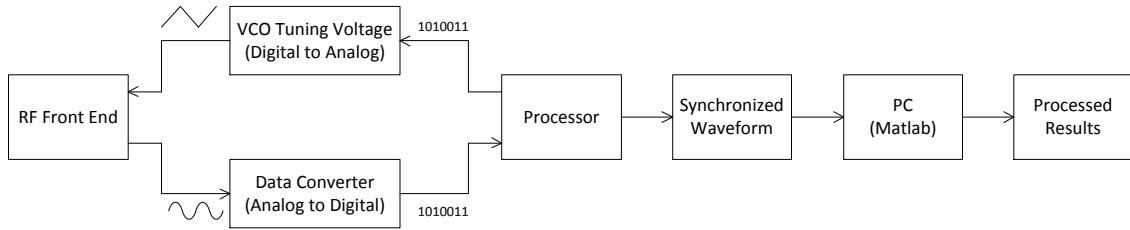


Figure 4.1: System Block Diagram

4.2 A RADAR Prototyping Platform

The ultimate objective was to allow the development platform to provide environmental information to an automotive control system capable of increasing fuel efficiency. By designing the radar system with the application of an automotive control algorithm in mind, there is potential to produce a sensor that is not only better suited for the application, but is also more affordable.

4.2.1 Platform Requirements

The design approach which has been used throughout this project was a piece-wise approach. Rather than jumping straight into trying to develop a completely embedded system everything from the RF components to the RADAR data processing, everything will be done in small steps. To help design the data processing algorithms, raw data is first needed to be analyzed. The approach taken was to capture it and bring it directly into a mathematical analysis program like MATLAB to design the required processing algorithms. This requires the platform to have the ability of acquiring large amounts of data in real time on a PC. Additionally the platform must not only allow prototyping of the required signal processing algorithms, but should also allow the ability to implement the algorithm in an embedded fashion (i.e., on a DSP for example). Having the ability to embed the algorithm in the prototype platform allows for the potential of providing real-time data to a powertrain control system to verify the tradeoff assumptions with real experimental data.

The overall system will consist of both RF and digital components capable of performing distance and velocity measurements. The combined system will be capable of generating

a radar signal, measure reflections, and then process the information to determine system outputs.

The platform will be broken into two main components. The first component is the digital subsystem. This will be described in full detail within section 4.2.2. The second main component is the analog and RF subsystem. This will be described in full detail within section 4.2.2. The conceptual approach taken within this project will be to design the system using a modular approach, so the work done may be used in later projects for other further experiments. As a result of this approach, the digital subsystem and RF subsystems will be designed and manufactured as two separate modules which will ultimately interface with each other to complete the system. The approach of two independent PCBs which through a connector interface would allow signal sharing has the advantage of using different PCB manufacturing processes for the RF portions vs the digital portions.

The main purpose of the digital subsystem is to provide all necessary support (power, data-conversion, data processing, input/output interfaces, debugging, and testing). It may provide stimulus inputs to the RF subsystem, and it will also receive outputs which will contain information to be processed.

The main purpose of the RF subsystem is to provide all RF functionality (antenna, VCO, mixers, signal-chain, etc). It will take inputs from the digital subsystem (such as a DAC generated input to the VCO), and provide an analog baseband signal for which contains the desired information to be processed.

4.2.2 Hardware

The physical hardware may be broken down into two subsystems. The first subsystem is a digital subsystem consisting of all digital computing and processing. The second subsystem is an analog and RF subsystem which will consist of all required analog power, signal filtering/conditioning, and RF support. The two subsystems will be combined and built on a printed circuit board.

Digital Subsystem

The digital subsystem is made up of a microcontroller, a digital signal processor, and a FPGA. All three components are connected together, such that they can share information. The microcontroller selected was an STM32F2 ARM Cortex-M3 based device [14]. The DSP selected was an Analog Devices Blackfin BF518-F device [15]. The FPGA selected was an Altera Cyclone III EP3S25 device [16].

The purpose of the microcontroller is to facilitate the operation of the system master. The microcontroller's main application consists of a custom USB device protocol stack which responds to commands transmitted by the host. When connected to a PC host, commands can be sent through software to configure and control the development platform. The microcontroller is not designed to any processing of the data, it is mainly responsible for moving data around the system.

The purpose of the digital signal processor is to handle the raw data processing. At this initial stage of the project, the DSP does not have a processing algorithm running, but instead it outputs the raw unprocessed data to the microcontroller. At the time the algorithm development is complete, the processing algorithm may execute on this device. Implementing the algorithm on the DSP provides the simplest method of embedding the algorithm and running it in real time on the system.

The purpose of the FPGA is to provide an additional lower level option to prototype parts of the processing algorithm. The FPGA provides the ability to implement all or sections of the algorithm at the [RTL](#) level. By using an FPGA for this level of prototyping, it brings the system one step closer to being able to be a fully embedded ASIC capable of performing the desired processing.

Analog and RF Subsystem

For the RF subsystem, rather than building everything from scratch, an off the shelf module which is commercially available was selected. This module consisted of all components integrated within a nice form factor package. The module was designed by RFbeam (<http://www.rfbeam.com>). The module selected was the K-MC4 radar transceiver. All documentation including a block diagram is available online [\[17\]](#).

This module provides a two channel [IQ receiver](#), with both transmit and receive antenna. The module provides a bandwidth of approximately 250 MHz starting at 24.0 GHz.

Platform Hardware Design

The full design from schematic to layout was completed for the purposes of this project. The schematic entry and layout was done using EAGLE cad software v5.1 for Linux. The design was a 6-layer PCB, which consisted of a solid ground plane, a power plane (split up for different supplies), two internal routing layers, and a top/bottom for routing. For more details on the design, refer to [Appendix A](#).

4.2.3 Software

The software required to be developed consisted of embedded software and PC software. The embedded software executes on the microcontroller, DSP, and FPGA. The PC software executes on the PC and communicates with the embedded software through a USB interface and custom protocol stack.

Embedded Software

The embedded software required to be developed for the prototyping system consists of all software running on the embedded microprocessors. For the purposes of the experimentation done to date, the [FPGA](#) has not been used. A standalone application was developed for both microcontroller and [DSP](#). Together the applications provided communication and the desired signal processing.

Microcontroller Firmware

The microcontroller software was the more complex program. Since the microcontroller was the system master, it was required to facilitate control of all components. The interface to the outside world was a high-speed USB device interface. The microcontroller software acted as a command handler, where commands were received over USB, then executed. In addition to the USB handler, the microcontroller contained the following functionality:

- USB device protocol for HID bulk transmission
- I2C / SPI master mode driver
- DSP to microcontroller parallel data interface
- RF module control interface
- ADC configuration and control
- PLL configuration and control
- DAC waveform generator
- Waveform / ADC synchronization from section [4.2.4](#)

The waveform / DAC synchronization described in section 4.2.4 was fully implemented as part of the microcontroller firmware. The waveform was generated using the DAC. For a low CPU overhead implementation, the DMA was used to transfer the table-defined waveform to the DAC. The rate of which the DMA transferred the next waveform sample was controlled by a timer. A timer was configured to count $\frac{N}{S}$ edges of the ADC clock, and once the defined ration was reached, it would trigger the DMA to transfer the next sample. This repeated indefinitely, with the table wrapping every period.

As the samples were received from the DSP, they were marked as either a rising edge sample, or a falling edge sample. This state was managed by a global variable that was updated every DMA interrupt, which would occur at the end of each rising or falling edge component. By marking the data in this way, it was possible to buffer it and transmit it to the PC for offline processing.

DSP Firmware

The DSP firmware was a rather simple application. The DSP interfaced directly with the ADC, and therefore received all the digital samples. The DSP firmware to this point did not contain any processing of the data, but rather transmitted each received sample directly to the microcontroller. This was done, since all the processing was required to be performed by the PC, as the processing algorithm was not as of yet defined.

PC Software

The PC software provided a way for the user to interact with the prototyping platform. To do this, the following PC software was developed (from lowest level to highest):

- USB HID-bulk mode drivers for windows
- DLL containing custom communication protocol functions
- C program calling DLL functions (for DLL debugging)
- Matlab wrapper for DLL
- Matlab scripts collecting / processing data

A DLL containing custom communication protocol functions was created, which allows a higher application layer program to call. The function interface is shown in Appendix B. Each of the functions will issue a command to the prototyping platform, which will instruct it to perform a specific operation, or return a specific result. Through this communication interface, the PC is able to interact and control the prototyping platform.

The most important component relevant to the experimentation at this stage is the MATLAB wrapper for the DLL. The wrapper functions are provided in Appendix C. These wrappers provides the ability for any function within the communication DLL to be called directly from a MATLAB script. This is a very powerful setup, because it combines the data acquisition and signal conditioning ability with the high level data processing capabilities of MATLAB. Using this concept, the radar system can be designed, tested, and optimized at a very high level through MATLAB. Then, as satisfactory results are obtained, the processing can be migrated piece by piece from MATLAB into the DSP, microcontroller, or FPGA.

4.2.4 Final Platform

The following figure illustrates the prototyping platform hardware with the variable gain amplifier and RF-beam K-MC4 radio module connected.

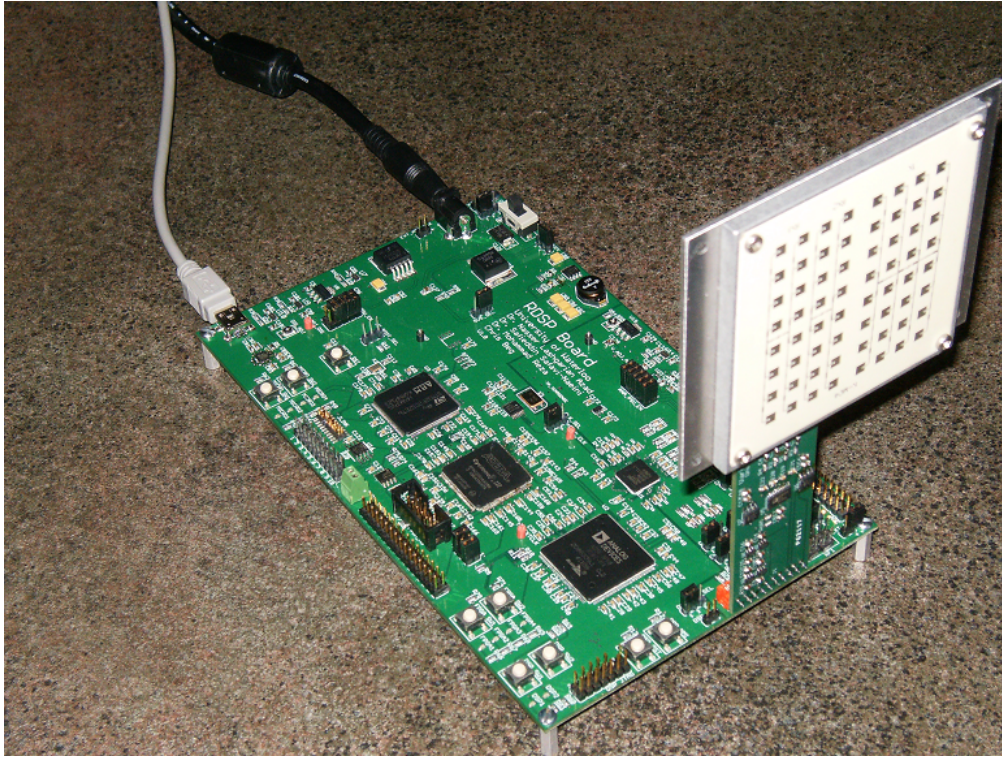


Figure 4.2: Prototyping Platform With RF Module

4.3 Realization of Baseband Optimizations

To facilitate the ability to tune the system as described in chapter 3, and to leverage the prototyping platform described in chapter 4, mapping of the functional blocks to subsystems will need to be performed. This chapter will describe how the system was implemented to allow testing and verification.

To start, figure 4.3 illustrates a top level view of the sensor system. It is made up of an RF subsystem, an analog and digital front end, a DFT (discrete Fourier transform). The remaining signal processing elements used to extract the encoded information are not covered within this analysis, as the processing subsystem is a larger study by itself.

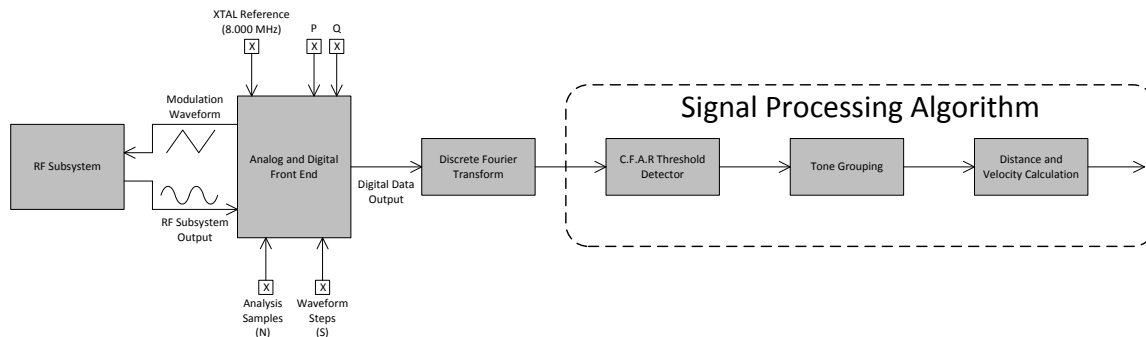


Figure 4.3: Top level architecture

As shown in figure 4.3, the analog and digital front end block has five additional inputs that are not connected to any other subsystem. These five inputs are an XTAL reference, and four variables labeled P, Q, N, and S. These five inputs are intended to provide easy control over the adjustment of the modulation waveform while not having to maintain any of the complex synchronization aspects. Through these controls, the waveform may be modified but the system will remain operating as expected to satisfy the constraints for the analysis outlined in chapter 3.

4.4 Realization Requirements

The following architecture was developed such that it would be possible to easily map the subsystem to either a microcontroller (STM32F2), or an RTL description for an FPGA. It was also developed such that it will be compatible with the prototyping platform.

The focus of the implementation will be the analog and digital front end as depicted in figure 4.3. Starting by examining the requirements for this subsystem, this block will be responsible primarily for synchronizing the modulation waveform with the analysis. To perform the synchronization, this block will be required to generate the modulating waveform so it has knowledge of the waveform state when performing the synchronization. Additionally, this block must be capable of configuring different sample rates and different analysis block sizes as described in chapter 3.

Since the modulation waveform may consist of possibly different shapes, it is desirable to be able to have this system capable of experimenting with other shapes aside from a triangular shape. The focus of this section will be using a triangular shape, however the

capability may be extended to other shapes at a future time. To facilitate this requirement, the approach taken will be to break the modulation waveform into discrete sections, or steps. The amplitude will be defined at each step of the waveform.

Shown in figure 4.4 below, the modulation waveform is to be broken up into S discrete steps. There are to be a total of N ADC samples taken. The only constraint on selecting N and S is that the ratio of N to S must be an integer.

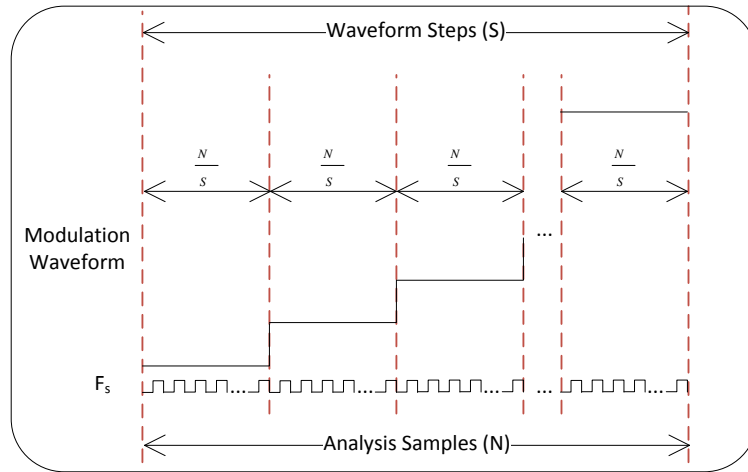


Figure 4.4: Resulting waveform and timing

4.5 Design Realization

The implementation of the analog and digital front end starts with the design decision that the block must be clocked by the same source as the ADC sample clock. By making this decision, it creates a level of synchronization that allows for the processing and waveform generation to be timed off the same clock source. The idea is based on the fact that the modulation waveform is updated on the negative edge of the ADC clock, and the ADC sample is generated on the positive edge.

As illustrated in figure 4.5, a block level depiction of the analog and digital front end is made up of a fractional PLL, an analog to digital converter, and a digital to analog converter. This block also consists of a modulation waveform generator block, and a sample collection block which will be described in more detail further below.

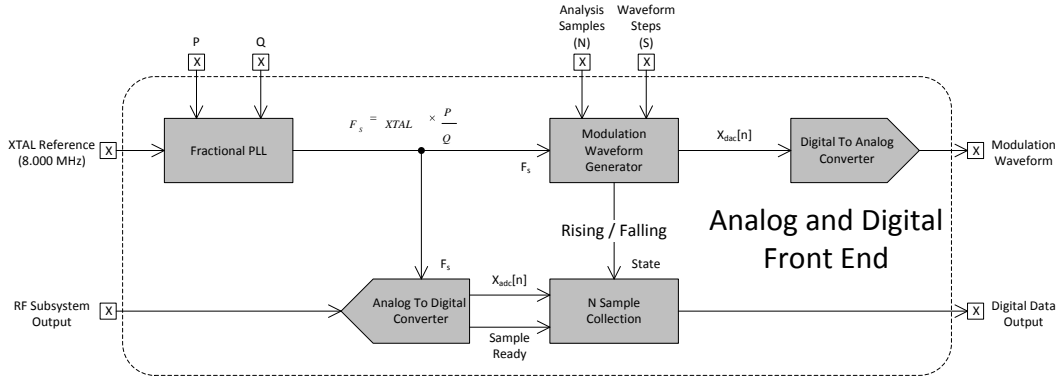


Figure 4.5: Analog and digital front end

The fractional PLL will be responsible for generating the ADC sample clock, which is the clock used to time the modulation waveform generation. This block will use a reference clock, and two variable inputs labeled P and Q. These two inputs will provide the fractional control for generating the desired ADC sample rate (F_s). The expression used to define the PLL's output frequency is given by equation 4.1.

$$F_s = XTAL \times \frac{P}{Q} \quad (4.1)$$

The analog to digital converter [ADC](#) is directly clocked with the PLL output (F_s). Every positive edge of the clock will prompt the converter to produce a new sample. The ADC will convert the baseband signal provided from the RF module. The converted sample is then provided to the sample collection block.

The digital to analog converter [DAC](#) will convert the digital output from the modulation waveform generator block into an analog representation. The modulation waveform generator block is clocked from the same clock as the ADC, and as a result will be synchronous to the ADC.

Illustrated in figure 4.6 below is the contents of the modulation waveform generator. This subsystem is clocked by the ADC clock F_s , and will output updated samples for the DAC to reproduce the modulation waveform. As control or tuning inputs, this block will be provided with the N and S variables. This block will also produce a state output, which will be provided to the sample collection block and will indicate if the modulation waveform is in the [up-chirp](#) or [down-chirp](#) state.

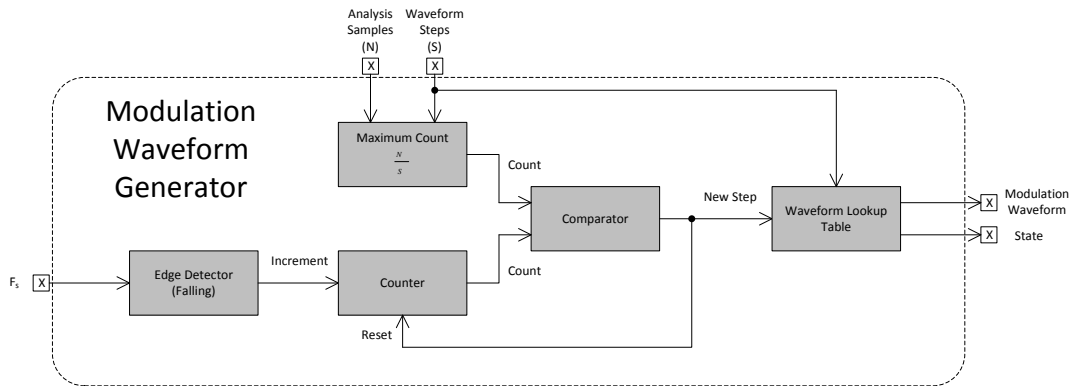


Figure 4.6: Waveform generator block

The operation of this block is not overly complex. Using the N and S variables, a maximum count per modulation waveform sample update is computed by dividing $\frac{N}{S}$. Next, a falling edge detector on the F_s clock will increment a counter, which will count up to $\frac{N}{S}$. Once the maximum count has been reached, it will be automatically reset, and trigger a new sample to be fetched from a modulation waveform lookup table.

Illustrated in figure 4.7 is the sample collection block. This block will be provided two control signals which indicate when a new sample is ready, and when there is a change in the the up-chirp or down-chirp state. Additionally, this block receives the sample from the ADC, and outputs a block of data to the DFT algorithm.

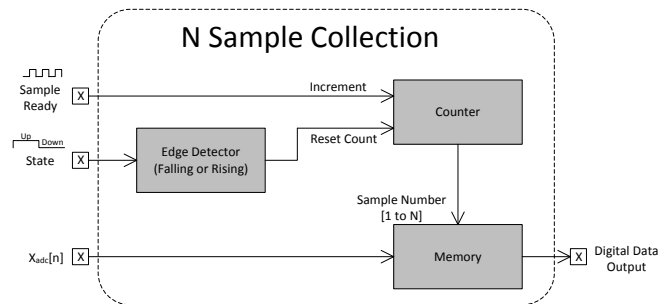


Figure 4.7: Sample Collection

The memory will contain N samples, all of which belong to the up-chirp or down-chirp portion of the modulation waveform. Together, the full system will remain synchronous,

and through adjusting the F_s frequency (using the three PLL inputs), the sampling frequency may be adjusted. Through tuning of the N variable, the number of samples for each analysis block may be adjusted. Finally, through the S parameter, the quantization of the modulation waveform can be adjusted.

Chapter 5

Field and Lab Measurement Results

5.1 Verification

To verify the results of the analysis, it is desirable to link the theory and analysis to actual field measurement results. As a verification to the analysis and tuning presented in this thesis, an actual system consisting of the calculated parameters will be analyzed and tested in the field to correlate the calculations with the physical environment.

To begin with the verification, the sensor will be tuned to meet a specific set of specifications. Measurements will be done to verify the tuning is accurate. Once the tuning is calibrated to known state, the system will be brought into the field to perform measurements.

At this stage, only distance measurements will be performed. Measuring a relative velocity is difficult, as a consistent and reproducible setup allowing for measuring accurate velocities at different ranges will need to be created. Building such a setup is outside the scope of this thesis, and will be left as a future exercise.

The distance measurements will be performed in an empty parking lot where large distances can be measured. In measuring distances, there are still many sources of error involved when measuring distances, such as angle (or line-of-sight) to the target and accuracy of measurement to the target.

A verification of the system will be considered complete if it is possible to calculate and predict the location of the majority of the received signal energy corresponding to a measured physical distance.

5.2 System Setup

The prototyping platform was configured and setup as described in section 4.2.4, where the available tuning parameters were a reference clock (8.000 MHz), and described system variables [N, P, Q, and S]. For reference, the configuration is illustrated in figure 4.3. The RF front end used was the K-MC4 module designed by RFBeam, and is described in the datasheet [17].

Before verifying the system, some measurements were necessary to characterize the RF module. Given in the K-MC4 datasheet is the approximate VCO output frequency with respect to VCO tuning voltage. This curve is also illustrated in figure 5.1, as found in [17, Fig.4]. Up until now, it was assumed that the VCO provided a tunable bandwidth of 250 MHz, however to obtain accurate results, this has to be measured and understood.

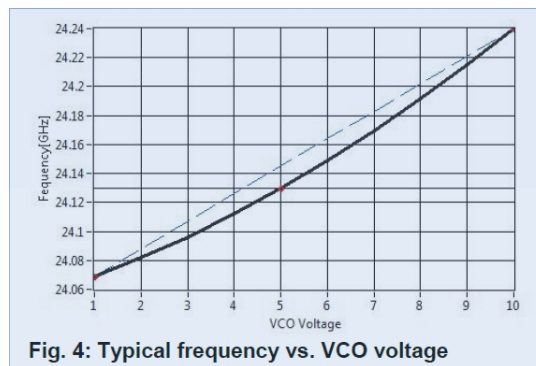
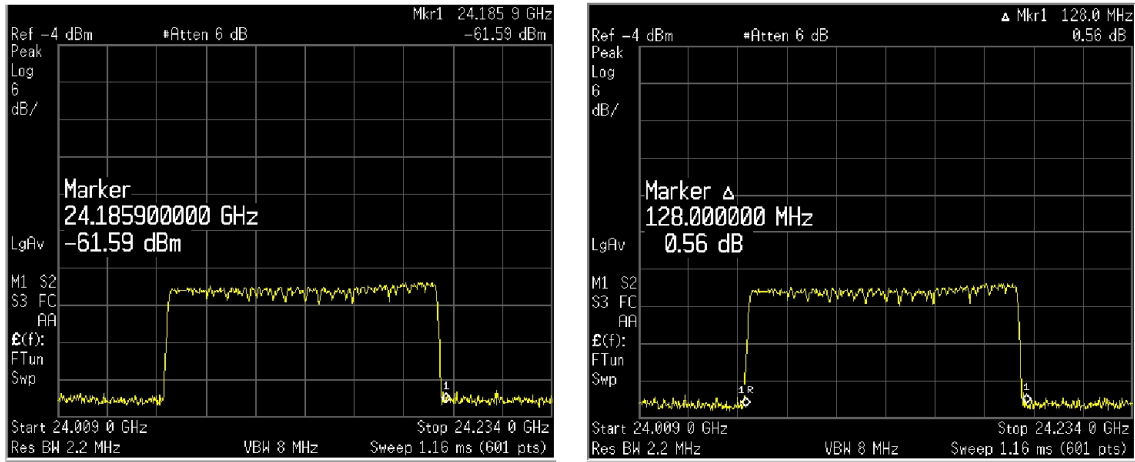


Figure 5.1: RFBeam K-MC4 Module VCO Tuning

To measure the module's bandwidth, a 10 volt VCO tuning range was used. The tuning voltage was swept from 60 mV to 10.06 V. The resulting frequency output of the module was measured at the modules transmit antenna, with a spectrum analyzer. Figure 5.2(a) shows that the upper frequency output of the module with a 10.06 V input is approximately 24.1859 GHz. Figure 5.2(b) shows that the RF bandwidth given the tuning range of 60 mV to 10.06 V is approximately 128.000 MHz.



(a) Module Upper RF Frequency Measurement

(b) Module RF Bandwidth Measurement

Figure 5.2: RF Measurements

Keeping the same system requirements outlined in chapter 3 as shown in table 3.1 (System Specifications), and given the actual RF bandwidth and center frequency measurements of the module, the system will need to be tuned. The tuning procedure described in chapter 3 was applied, and N was selected as 2048. The resulting system tuning specifications and requirements as per the tuning procedure are shown in table 5.1.

Table 5.1: System Tuning Specifications and Requirements

Parameter	Value	Units
Minimum RF VCO Frequency	24.0579	GHz
Maximum RF VCO Frequency	24.1859	GHz
Δf	128.000	MHz
f_{avg}	24.1219	GHz
c	3.00000×10^8	m/s
ΔV_{max} (relative)	83.3333 (300.000)	m/s (km/h)
Δd_{max}	250.000	m
N	2048	samples
Expected F_s (equation 3.2d)	33.855	ksps
T (modulating waveform chirp period)	60.492	ms

The specifications are the required parameters to map the system tuning onto a real system, as described in chapter 4.2.4. The resulting tuning is fully summarized in table 5.2 below. Note that since the K-MC4 module has a four channel output, the system was adjusted so all four outputs can be sampled. This required the ADC to run 4x faster, and that is reflected in the ADC clock being 4x faster.

Table 5.2: System Tuning Realization Parameters

Parameter	Value	Units
Frequency Reference	8.00000	MHz
N	2048	samples
P	82	Constant integer
Q	4844	Constant integer
S	4	Constant integer
Resulting ADC clock	135.425	kHz
Resulting F_s	33.856	ksps
Resulting T (modulating waveform chirp period)	60.490	ms

5.3 Lab Measurements of System Setup

By configuring the prototype system with the parameters defined in table 5.1, measurements can be conducted to ensure the platform is working as expected. As described in the realization section, there are mainly two signals which need to be adjusted, and that is the ADC clock, and the modulation waveform.

The ADC clock frequency was measured using an oscilloscope. The measurement taken from the oscilloscope is shown in figure 5.3. The ADC clock frequency is expected to be 4x faster than the calculated sample rate, because all four channels of the K-MC4 module are being converted. The expected frequency is 135.425 kHz, and the measured frequency is 135.428 kHz, as shown in the bottom right as $1/\Delta X$.

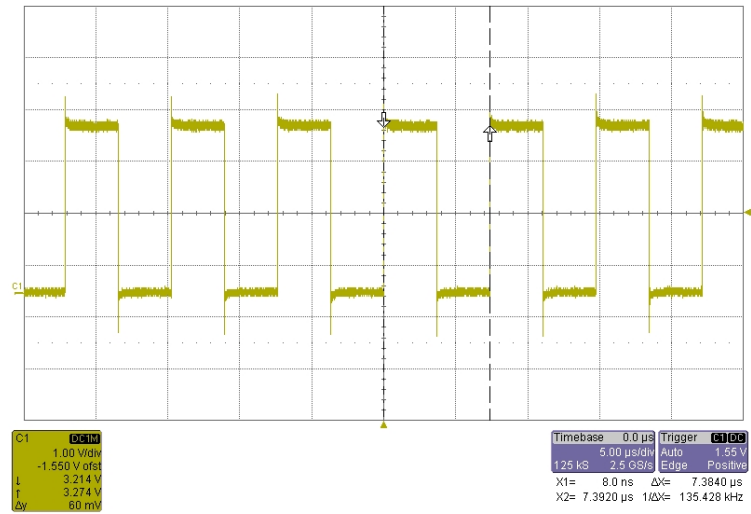


Figure 5.3: ADC Clock (4x clock)

The up-chirp time period was also measured using an oscilloscope. The measurement taken from the oscilloscope is shown in figure 5.4. The time period is expected to be 60.490 ms, and the measured time period is 60.485 ms, as shown in the bottom right as ΔX .

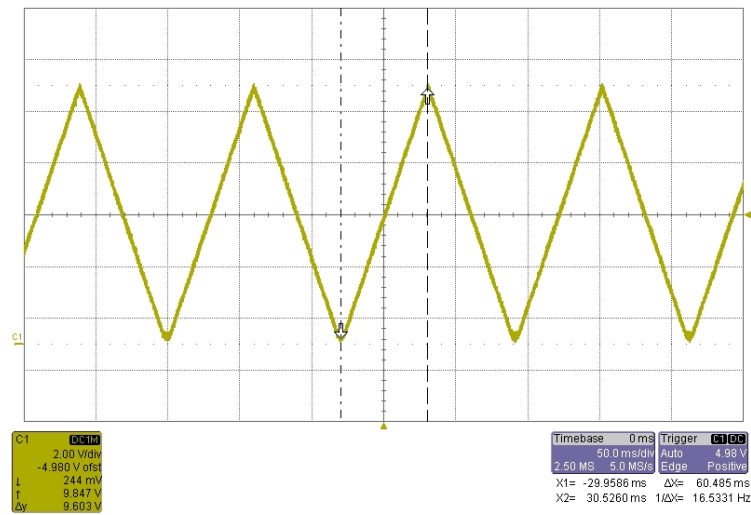


Figure 5.4: Modulating Waveform Up-Chirp Period

The down-chirp time period was also measured using an oscilloscope. The measurement taken from the oscilloscope is shown in figure 5.5. The time period is expected to be 60.490 ms, and the measured time period is 60.485 ms, as shown in the bottom right as ΔX .

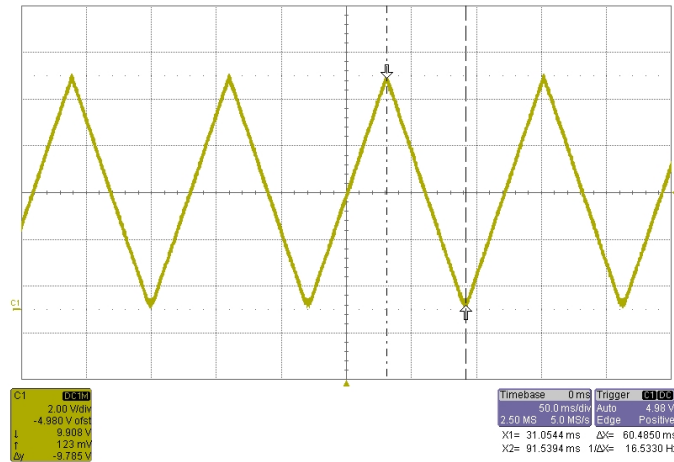


Figure 5.5: Modulating Waveform Down-Chirp Period

The RF bandwidth was defined as approximately 128 MHz, and was generated with a waveform amplitude of 60 mV to 10.06 mV. A measurement of the amplitude was taken using an oscilloscope. The measurement shown in figure 5.6 confirms the desired values.

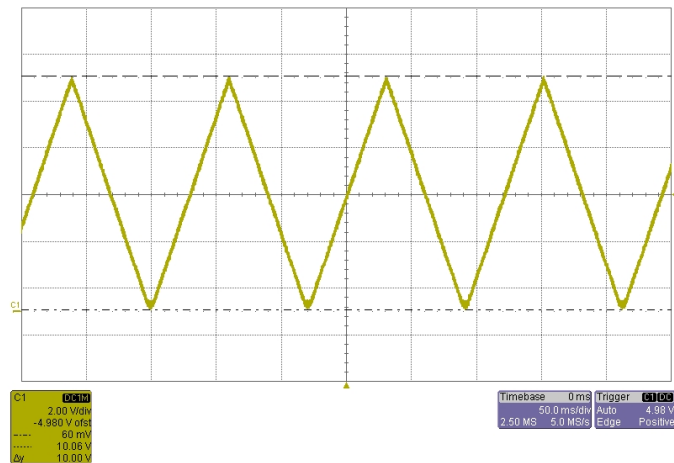


Figure 5.6: Modulating Waveform Amplitude

5.4 Theoretical Analysis of Expected Results

Given the system tuning described, the theory derived in section 2.5.2 will be used to provide an expected outcome of the system. Equations 2.20a and 2.21a were used to calculate the expected output.

Illustrated in figure 5.7 below is the expected result for a stationary object located 40m away from the sensor.

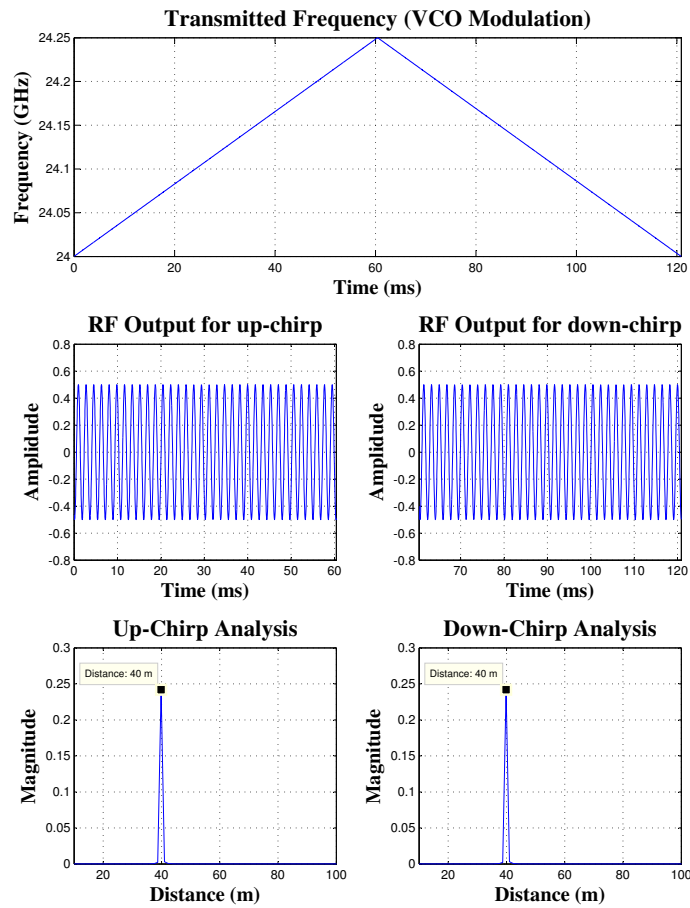


Figure 5.7: 40m theoretical result

The upper plot illustrates the modulating waveform exactly as measured. The middle two plots illustrate the RF module baseband output as a result of both up-chirp and down-chirp events. The bottom two plots illustrate a frequency analysis, with the results scaled to distance. The relationship which will map a distance to a frequency is given by: $d(f) = f \times \frac{c}{4 \times \Delta f \times f_{tune}}$. As expected, since there is no Doppler shift, both up and down chirp events produce a distance of exactly 40 m.

Illustrated in figure 5.8 below is the expected result for a stationary object located 80m away from the sensor.

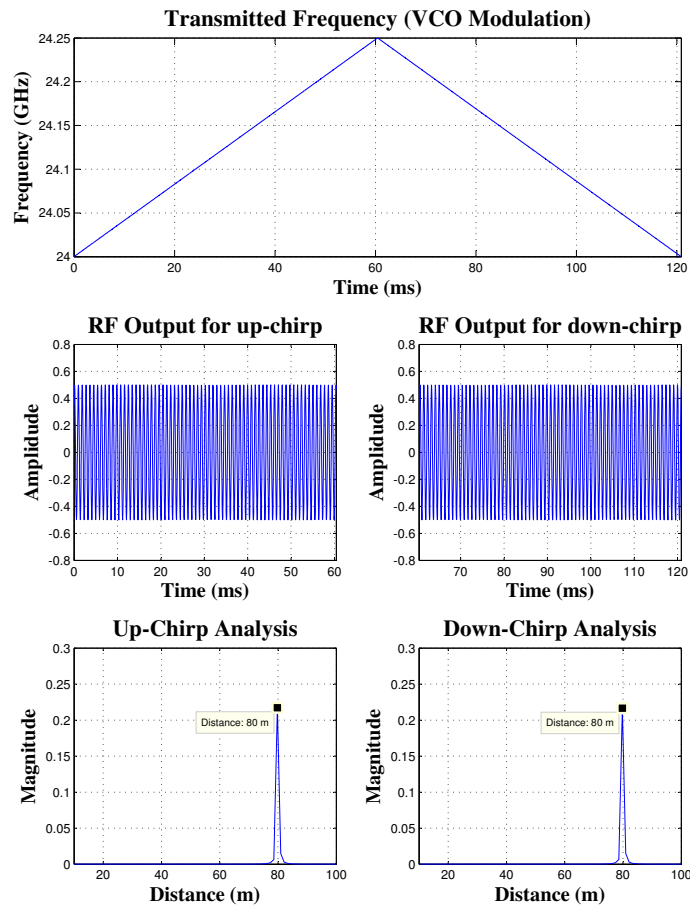


Figure 5.8: 80m theoretical result

5.5 Field Measurements System

Finally, to complete the verification, real measurements were performed using the prototyping platform. The measurements shown are expected to match those shown in figures 5.7 and 5.8.

Illustrated in figure 5.9 below is the actual measurement of an object located 40m away from the sensor.

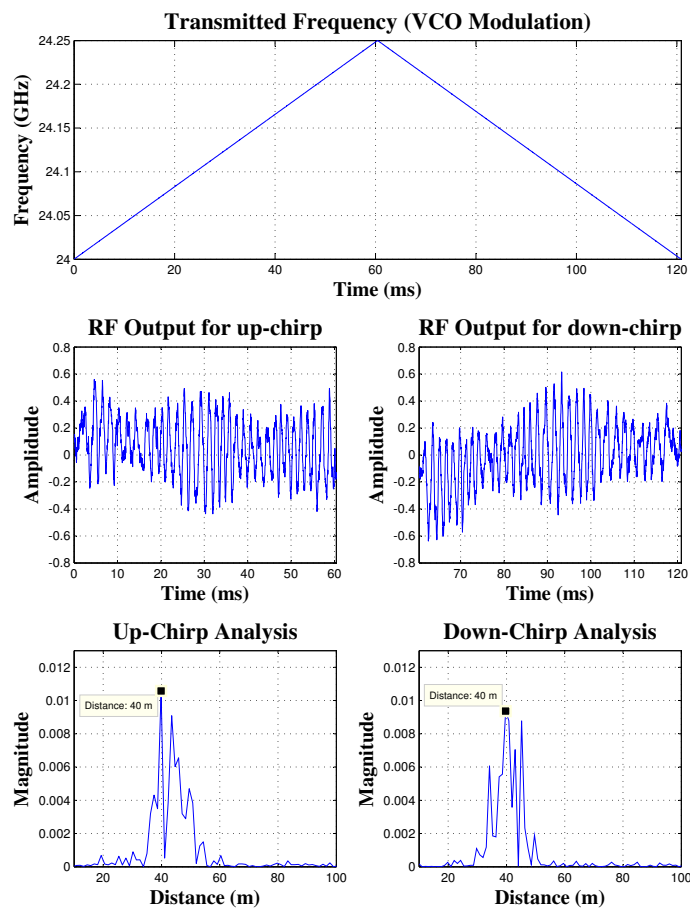


Figure 5.9: 40m measurement

Illustrated in figure 5.10 below is the actual measurement of an object located 80m away from the sensor.

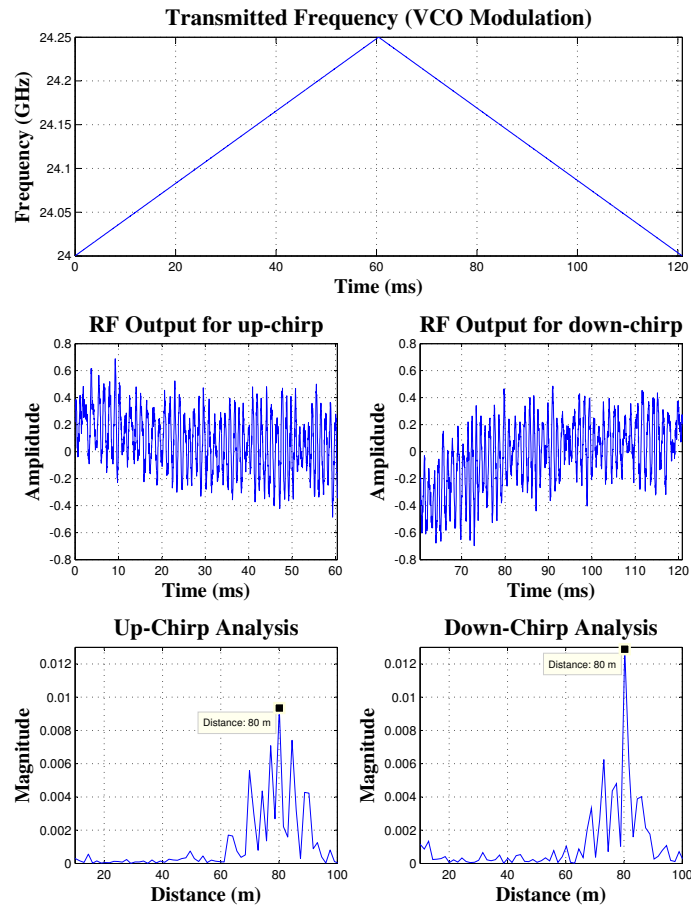


Figure 5.10: 80m measurement

The measurements presented here were obtained in an empty parking lot, and the distances were measured using a meter stick.

The theory discussed in the previous sections was taken into consideration and the optimization scheme presented in section Radar Sensor System Parameter Optimization.

Radar Sensor System Parameter Optimization was applied to obtain the system tuning. The platform discussed in section Radar Sensor Development Platform. Radar Sensor Development Platform was designed and manufactured, and used to realize the desired system parameters. Both the theoretical and experimentation results match very closely.

Chapter 6

Conclusions

Given the scope of the work done for this thesis, the objective was to design a low cost **RADAR** sensor for an automotive powertrain control application. To obtain a low cost solution, a **FMCW** architecture was selected due to the simplicity of the **RF** and baseband components.

6.1 Modulation Waveform Comparison

The model of the three commonly used modulation waveforms were derived and studied. The three waveforms analyzed were sawtooth, triangular, and sinusoidal shapes. Each waveform has advantages and disadvantages when compared to each other, and different ways of encoding information.

The sawtooth waveform provided a way to measure distance. The measurement result is encoded as a frequency in the baseband output. However, the measurement information contains a combination of delay (distance) and **Doppler** shift (velocity). The waveform does not provide a convenient way to separate the two components. The separation will have to be done in the baseband processing, where multiple measurements would need to be examined and then an observation of how the result changes over time would allow an estimate of the object distance and velocity to be approximated.

The triangular waveform is an extension to the sawtooth waveform, where the measurement is broken into two sub-measurements consisting of a positive and negative slope. Also like the sawtooth waveform, the measurement result is encoded as a frequency in the baseband output. The advantage to the triangular waveform over the sawtooth waveform

is a built in mechanism exists to extract the delay component (distance) from the [Doppler](#) shift component (velocity). This is done by examining the result of both sub-measurements independently. The disadvantage of the triangular waveform over the sawtooth is it takes twice as long to perform a single measurement.

The sinusoidal waveform provides a way to measure both distance and velocity.

6.2 Baseband Optimizations

The baseband optimization section provided a guide for tuning the system for the application specific sensor designed for the powertrain control application described in this thesis. The baseband optimization attempts to balance bandwidth and processing requirements to reduce the complexity of the sensor, and hence reduce the cost.

The tuning also creates a level of synchronization between the transmitted waveform and the data processing. This synchronization creates a simple way to extract the desired data without a complex algorithm to match tone pairs.

This optimization was the basis for a conference paper published and presented during the IEEE ITSC 2012 automotive conference.

6.3 Realization

The realization section of the thesis focused on how the optimized sensor may be realized in an actual system. The realization described allows for an easily tunable system to adjust for different criteria as described in the baseband optimization section.

The realization started as a theoretical design, but was implemented on the prototyping platform and verified with actual measurement results.

6.4 Prototyping Platform

A prototyping platform consisting of hardware and software was developed to verify the theory and validate the optimizations recommended within this thesis. The realization section described a design which was implemented on the platform and allowed for measurements to be performed to verify the analysis performed.

6.5 Future Work

The experimental results section provides some real data as a step to confirming the optimizations are valid. Up until this point, the data collected has only taken place in a lab environment, making it difficult to fully test the maximum range and velocity parameters. In addition, factors like RF free space loss, and noise will be analyzed as the maximum limits of the sensor are stressed. Other potential issues to investigate include multi-sensor interference.

As the experimental results begin to strengthen, a more suitable real-time processing algorithm can be developed capable of providing input to the automotive control system. As a last step, the data and techniques presented here will be used develop and contribute to providing more energy efficient [HEVs](#).

Additionally, if this system is to be used as a product in an automotive application, the sensor will need to work in an environment where multiple sensors can work together. Since the [FMCW](#) architecture requires continuous use the [RF](#) spectrum, only one sensor can use the spectrum at a time. This is one advantage of pulse based RADAR systems, however they require very large bandwidths.

To get around the multiple sensor problem, there are a few ideas for enabling spectrum sharing. One option is a time-division multiplexing scheme, where each sensor operates for a small number of cycles, and then stops to allow a different sensor access to the spectrum. Another idea is a channelization method, where a block of spectrum is divided into different channels, where the sensor will select a free channel.

Both of these methods will require possible minor modifications to the RF subsystem, as the system will be required to detect activity on the spectrum. Additionally, some baseband logic will need to be added to allow for either different channel selection or performing the time division.

Finally, one more area for further research is to examine different modulation waveforms aside from the three examined within this thesis. Different waveforms may have the advantage of more optimal spectrum usage, by creating a system where distance and velocity is perhaps encoded in the phase or some other way. If a more optimal usage of the RF spectrum is obtained, the system becomes more ideal for a multiple sensor environment.

References

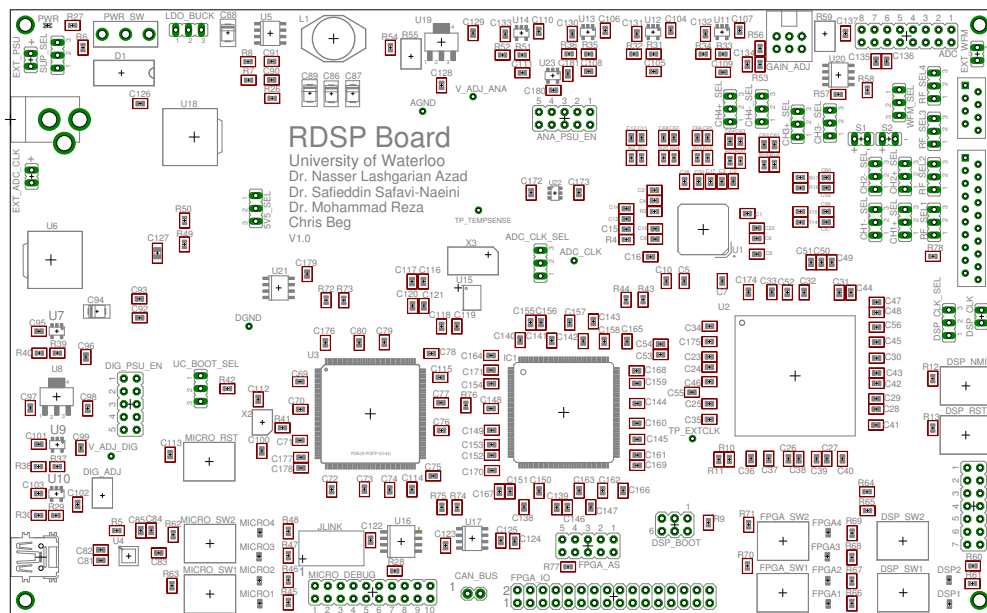
- [1] F. Flster, H. Rohling, and U. Lbbert, “An automotive radar network based on 77ghz fmcw sensors,” *Radar Conference, 2005 IEEE International*, 2005.
- [2] H. Dominik, “Short range radar status of uwb sensors and their applications,” *EuRAD Radar Conference*, 2007.
- [3] C. Schmid, R. Feger, C. Wagner, and A. Stelzer, “Design of a linear non-uniform antenna array for a 77-ghz mimo fmcw radar,” *IEEE MTT-S International Microwave Workshop on Wireless Sensing, Local Positioning, and RFID*, 2009.
- [4] E. Hyun, W. Oh, and J.-H. Lee, “Two-step moving target detection algorithm for automotive 77 ghz fmcw radar,” *IEEE 72nd Vehicular Technology Conference (VTC 2010-Fall)*, 2010.
- [5] W. Chang, L. Huan, and L. Yubai, “A practical fmcw radar signal processing method and its system implementation,” *International Conference on ITS Telecommunication Proceedings*, vol. 6th, 2006.
- [6] E. Hyun and J.-H. Lee, “Method to improve range and velocity error using de-interleaving and frequency interpolation for automotive fmcw radars,” *International Journal of Signal Processing, Image Processing and Pattern Recognition*, vol. 2nd, 2009.
- [7] H. Rohling and M. Meinecke, “Waveform design principles for automotive radar systems,” *CIE International Conference on RADAR*, 2001.
- [8] M. I. Skolnik, *Introduction to RADAR Systems*. New York, New York: McGraw-Hill Inc, second ed., 1980.
- [9] J. S. Seybold, *Introduction to RF Propagation*. Hoboken, New Jersey: John Wiley & Sons, first ed., 2005.

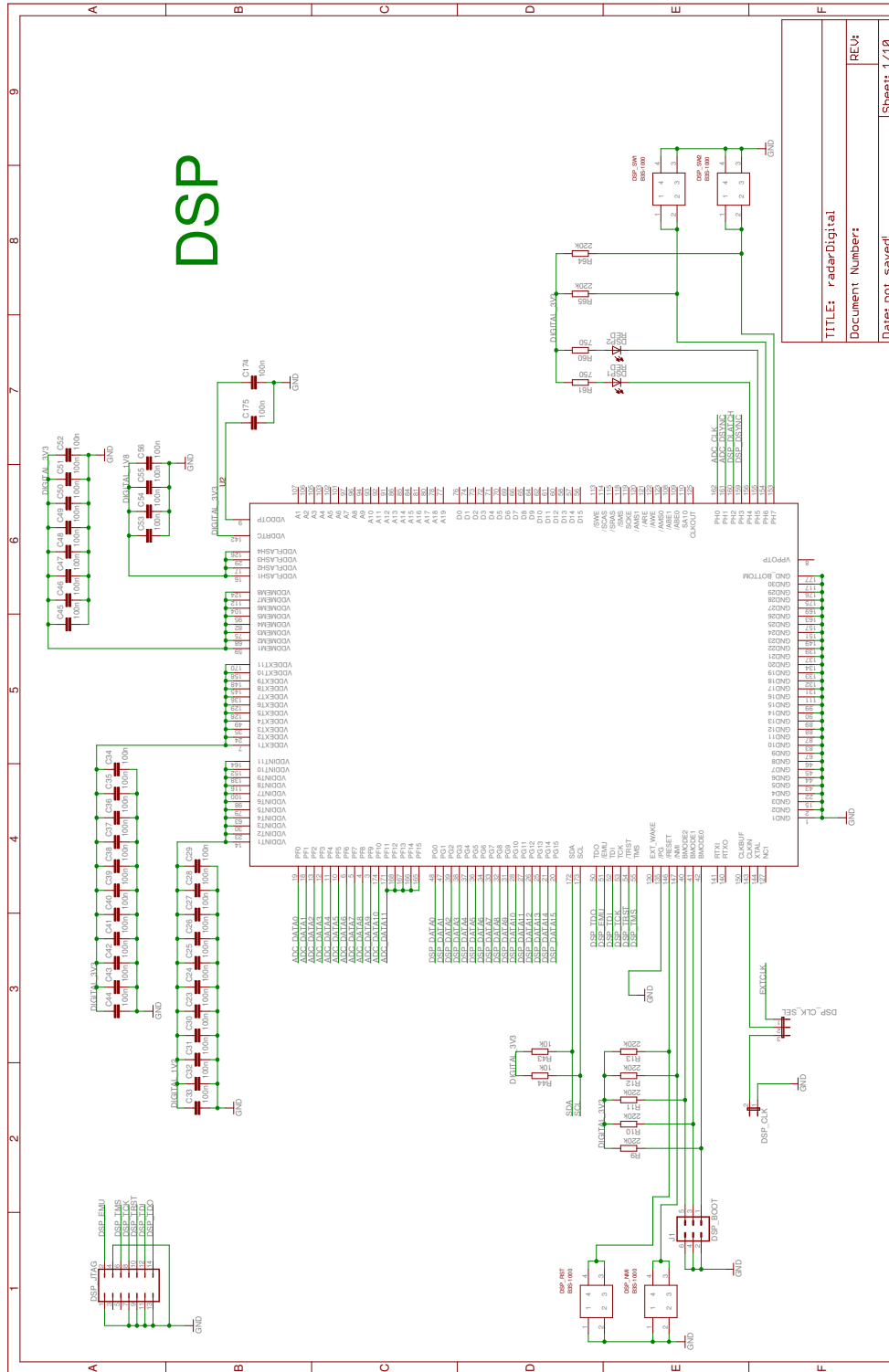
- [10] W. A. Davis, *Radio Frequency Circuit Design*. Hoboken, New Jersey: John Wiley & Sons, second ed., 2011.
- [11] J. Zheng, *Optical Frequency Modulated Continuous Wave Interferometry*. New York, New York: Springer, first ed., 2005.
- [12] C. Beg, M. Vajedi, M. Nezhad-Ahmadi, N. Azad, and S. Safavi-Naeini, "A cost-effective radar system for automotive powertrain control applications," *15th International IEEE Conference on Intelligent Transportation Systems (ITSC)*, 2012.
- [13] D. Sundararajan and M. O. Ahmad, "Matrix factorization derivation and analysis of computational complexity of a new radix-2 dft algorithm," *Circuits and Systems, 1996, IEEE Midwest symposium*, vol. 39nd, 1996.
- [14] S. Microelectronics, "STM32 F2 Hi-Performance - STMicroelectronics." <http://www.st.com/internet/mcu/subclass/1520.jsp>, 2012. [Online; accessed Oct-09-2012].
- [15] A. Devices, "ADSP-BF518F datasheet and product info." <http://www.analog.com/en/processors-dsp/blackfin/adsp-bf518f/products/product.html>, 2012. [Online; accessed Oct-09-2012].
- [16] Altera, "Cyclone III FPGA Family." <http://www.altera.com/devices/fpga/cyclone3/cy3-index.jsp>, 2012. [Online; accessed Oct-09-2012].
- [17] RFbeam, "RFbeam K-MC4 Radar Transceiver." <http://www.rfbeam.ch/products/k-mc4-transceiver/>, 2012. [Online; accessed Oct-09-2012].
- [18] F. G. Stremmer, *Introduction to Communication Systems, Third Edition*. Reading, Massachusetts: Addison-Wesley, 1992.
- [19] D. Halliday, R. Resnick, and J. Walker, *Fundamentals of Physics*. Hoboken, New Jersey: John Wiley & Sons, sixth ed., 2001.

APPENDICES

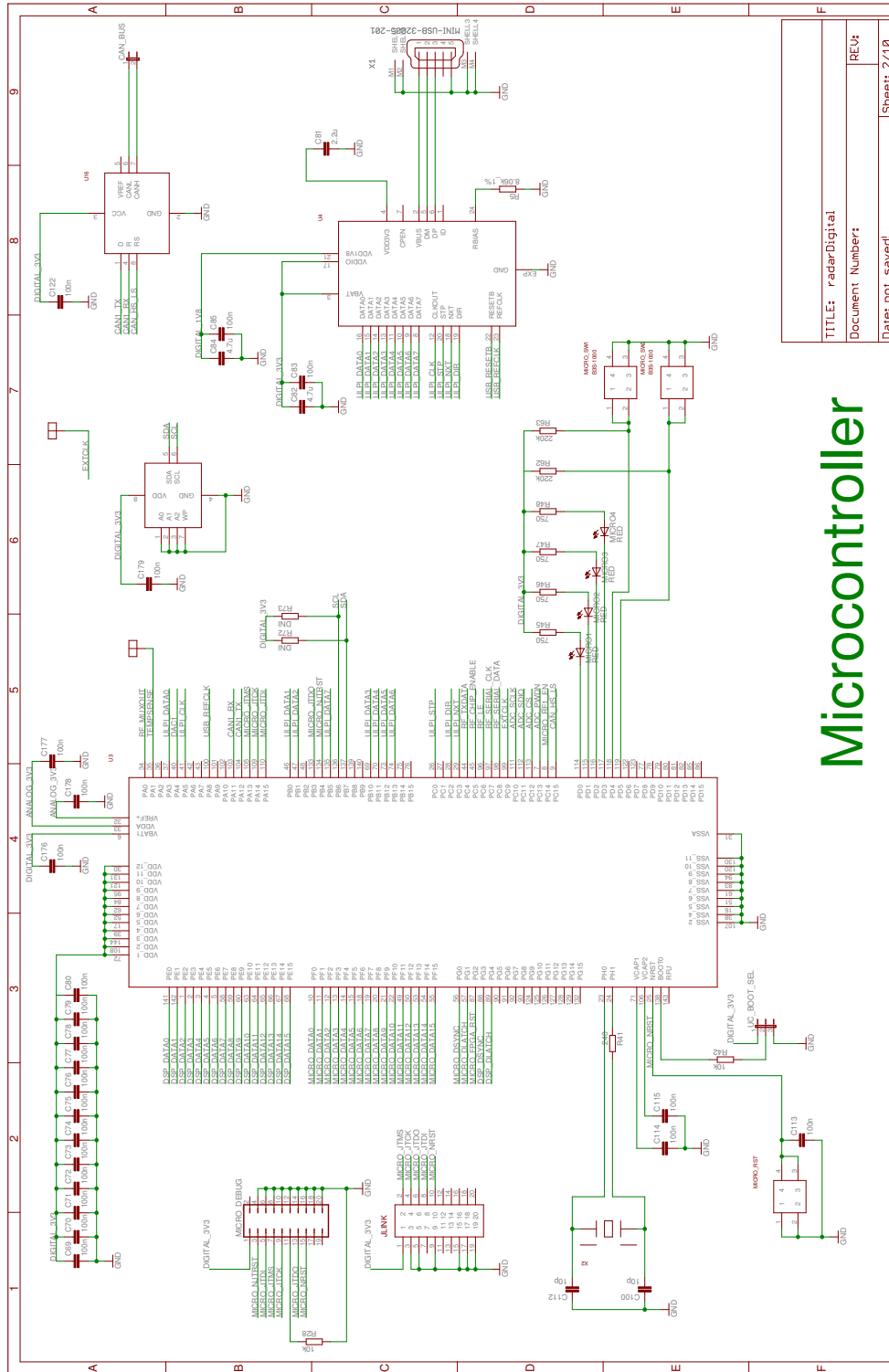
Appendix A

Prototyping Platform Schematics and Layout

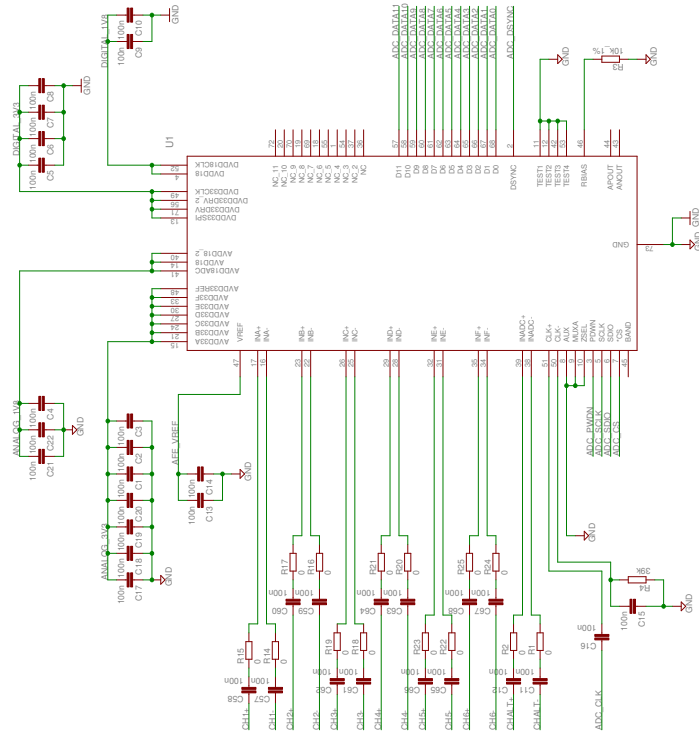




TITLE: radarDigital
 Document Number:
 Date: not saved!
 REU:
 Sheet: 1/10

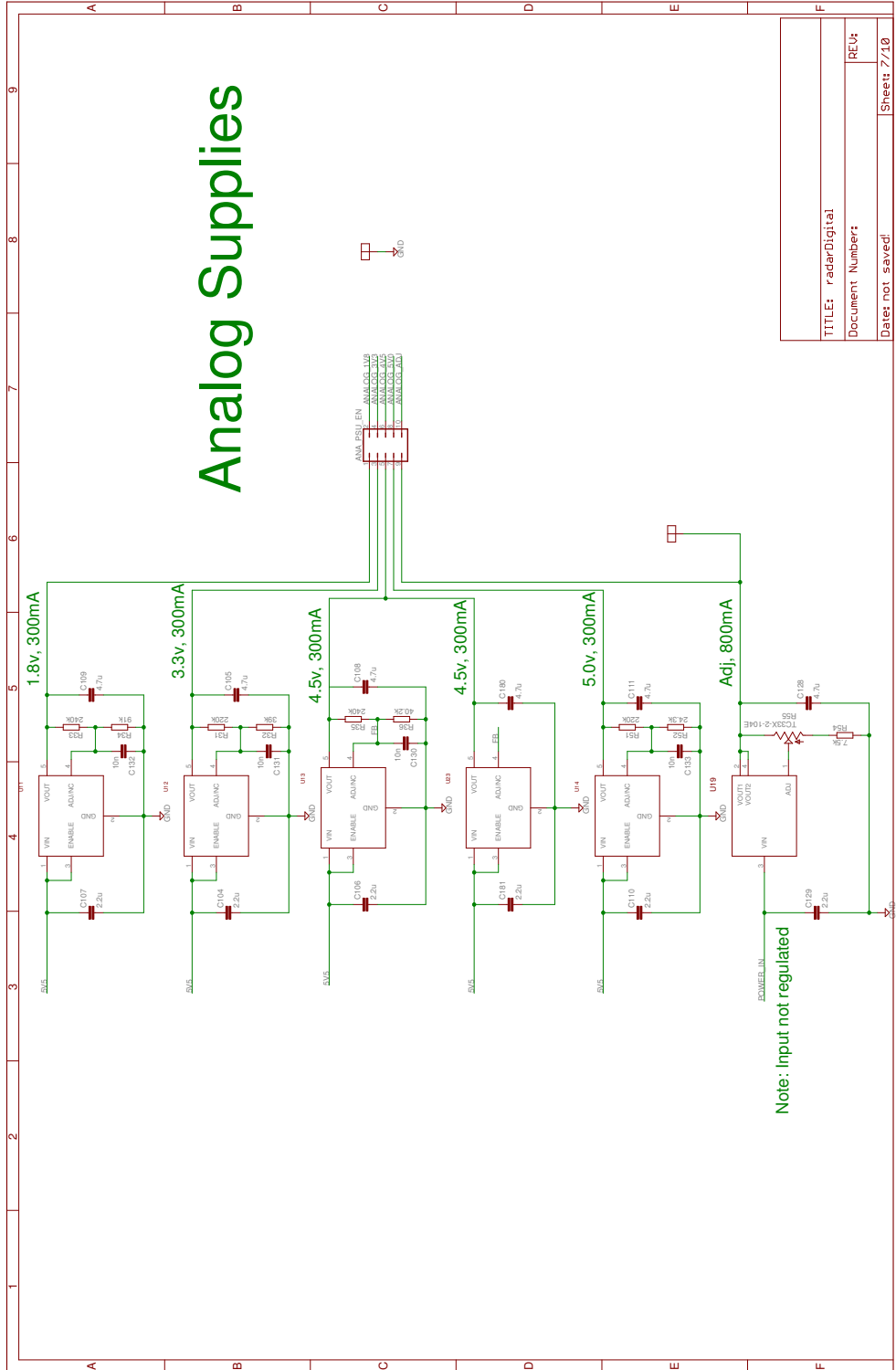


ADC



TITLE: radarDigital
Document Number: REU;
Date: not saved/ Sheet 4/10

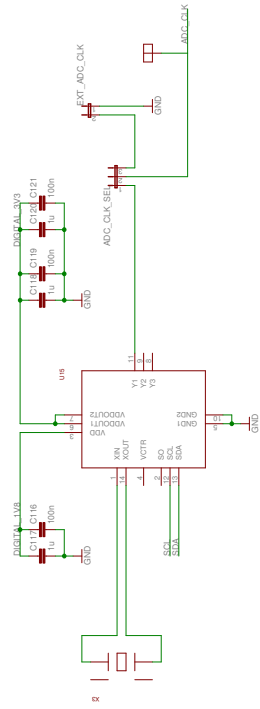
Analog Supplies



Note: input not regulated

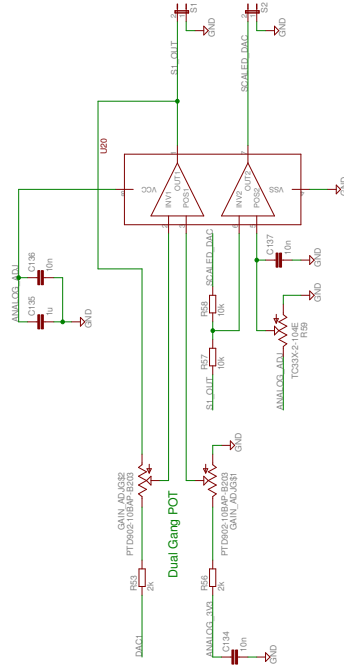
TITLE: radarDigital
Document Number: REU:
Date: not saved!

ADC Sample Clock PLL



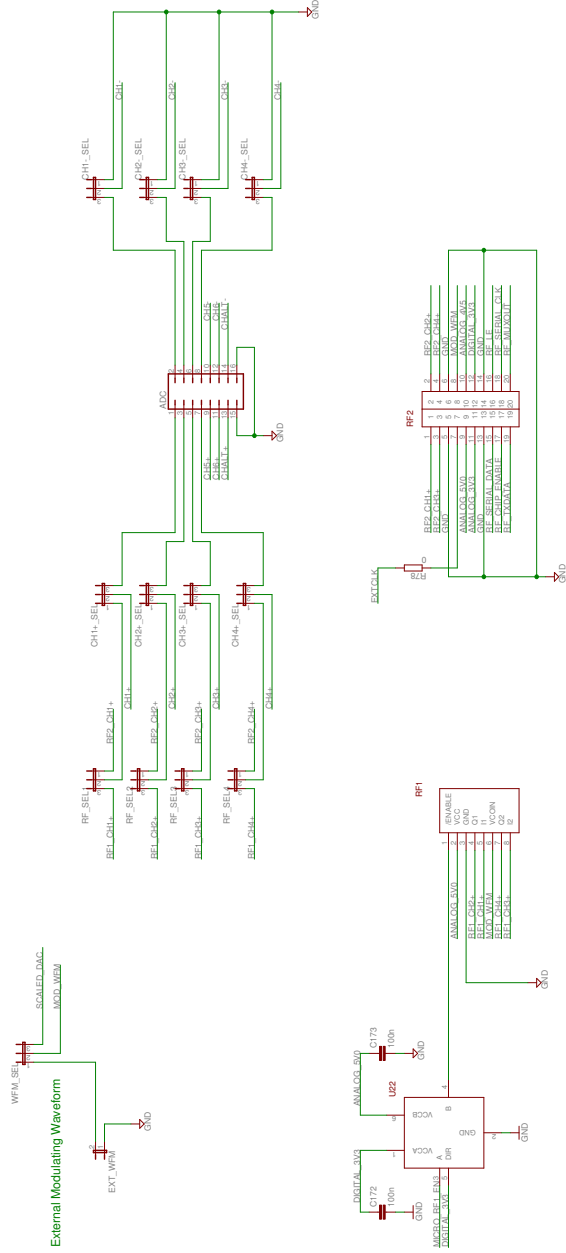
TITLE: radarDigital
Document Number: REU;
Date: not saved!

DAC Gain and Offset Scaling

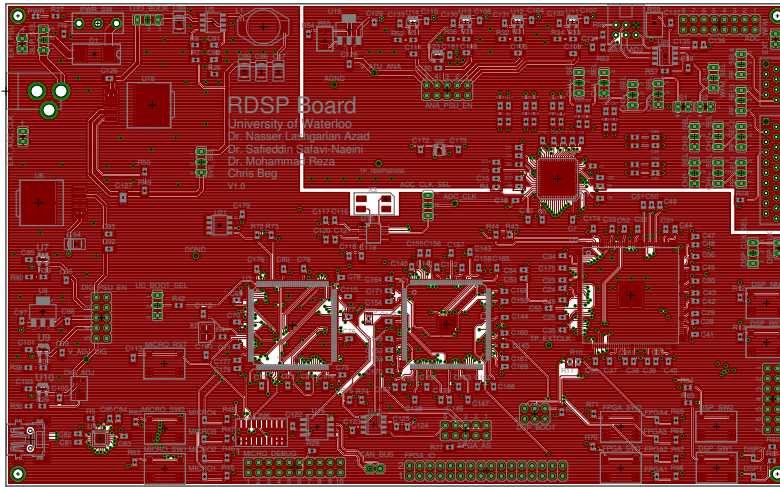


TITLE: radarDigital
Document Number: REU;
Date: not saved/ Sheet: 9/10

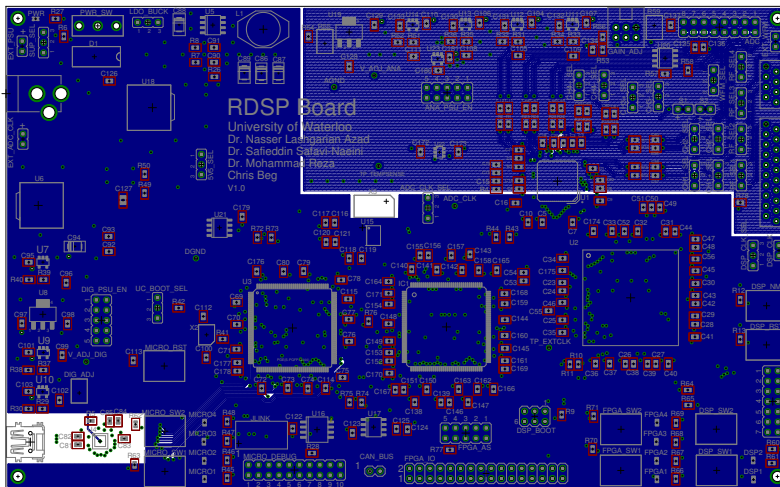
RF Connectors



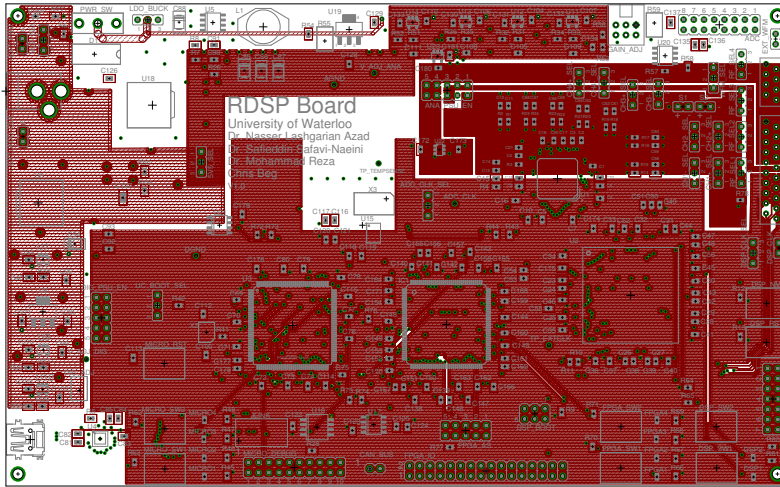
TITLE: radarDigital
Document Number: REU;
Date: not saved!



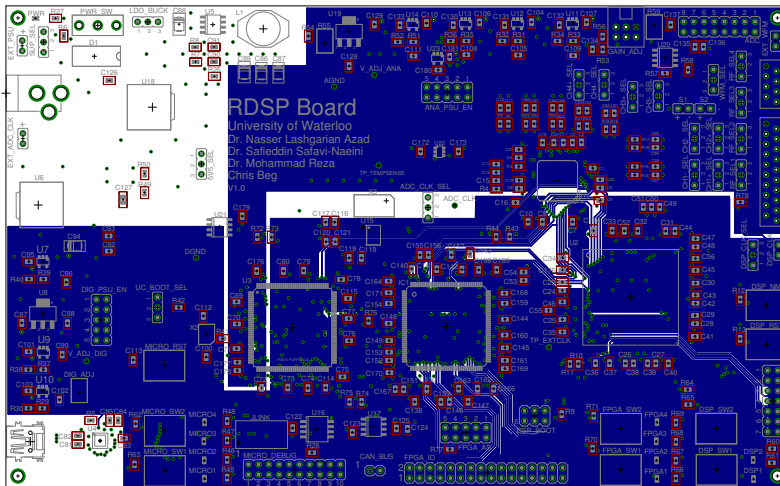
Layer 1



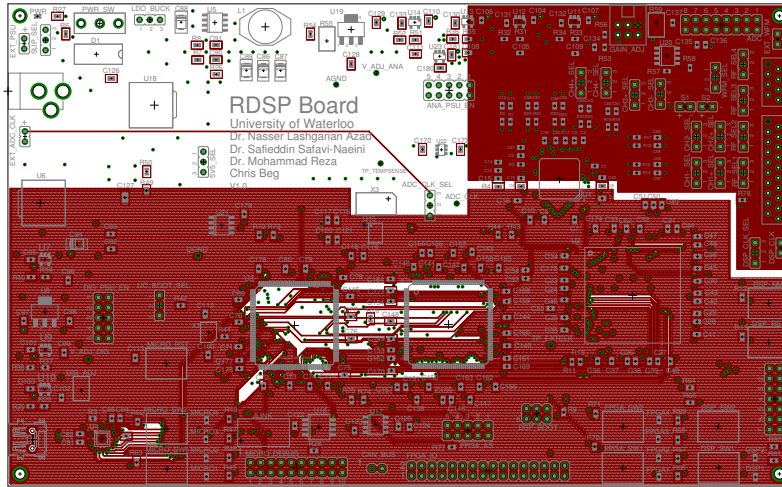
Layer 2



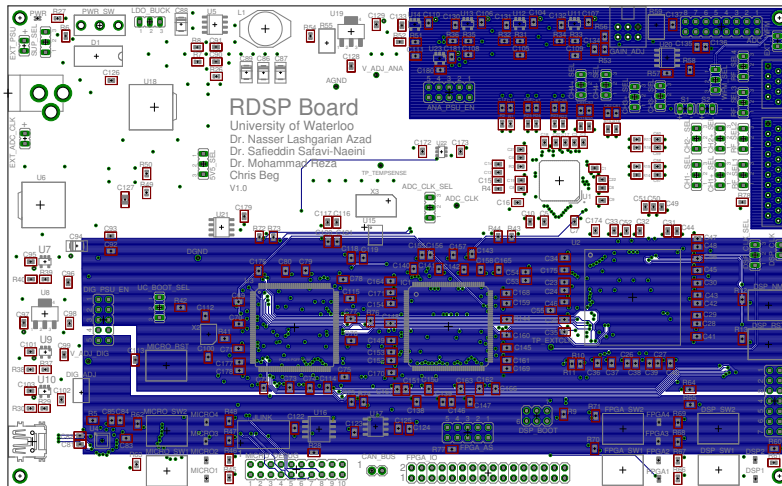
Layer 3



Layer 4



Layer 5



Layer 6

Appendix B

Prototyping Platform Communication DLL Interface

```
////////////////////////////////////
//          Internal Functions          //
////////////////////////////////////
#ifdef DLL_BUILD
    BOOL usbConnectionInit();
    void usbCloseConnection();
    BOOL waitForOperationComplete(ULONG msTimeout);
    int computeGCD(int p, int q);
    RDSPUSB_API BOOL __stdcall enableDisableADC(BYTE enable);
#endif

////////////////////////////////////
//          Exported Functions          //
////////////////////////////////////
RDSPUSB_API BOOL __stdcall isConnected();
RDSPUSB_API BYTE __stdcall getProtocolStatus();
RDSPUSB_API BOOL __stdcall setMicroLEDs(BYTE leds);
RDSPUSB_API BOOL __stdcall getMicroButtonStates(BYTE *button1, BYTE *button2);
RDSPUSB_API BOOL __stdcall programPLLWriteRegister(BYTE address, BYTE value);
RDSPUSB_API BOOL __stdcall programPLLReadRegister(BYTE address, BYTE *value);
RDSPUSB_API BOOL __stdcall programPLLWriteRegisterBlock(BYTE address, BYTE *registers, BYTE count);
RDSPUSB_API BOOL __stdcall programPLLFrequency(double xtalIn, int p, int q);
RDSPUSB_API BOOL __stdcall programPLLEnableOutput();
RDSPUSB_API BOOL __stdcall programPLLDisableOutput();
RDSPUSB_API BOOL __stdcall programPLLSaveToEEPROM();
RDSPUSB_API BOOL __stdcall disableADC();
RDSPUSB_API BOOL __stdcall enableADC(BYTE channels, BYTE gain, BYTE lpf);
RDSPUSB_API BOOL __stdcall receiveRealtimeADCData(short frames, short *data, short *dacState);
RDSPUSB_API BOOL __stdcall sendDSPCommand(BYTE command);
RDSPUSB_API BOOL __stdcall setVGAGain(BYTE gain);
RDSPUSB_API BOOL __stdcall setDACOutput(short outputCode);
RDSPUSB_API BOOL __stdcall setRFEnable(BYTE module, BYTE enable);
```


Appendix C

Matlab DLL Wrapper Functions

```
*****
% File Name      : rdspBoardLibraryOpen
% Author        : Chris Beg
% Version       : V1.0
% Date         : Feb-18-2012
% Description    : RDSP Board Library Open
*****
function [out] = rdspBoardLibraryOpen()
    if libisloaded('RDSPD11')
        out=1;
    else
        %PATH = './Software/RDSPD11/Debug';
        PATH = '.';

        LIBRARY = sprintf('%s/RDSPD11.dll', PATH);
        HEADER = sprintf('%s/RDSPD11.h', PATH);

        loadlibrary(LIBRARY, HEADER);

        if libisloaded('RDSPD11')
            out=1;
        else
            out=0;
        end
    end
end
end
```

```

%*****
% File Name      : rdspBoardLibraryClose
% Author        : Chris Beg
% Version       : V1.0
% Date         : Feb-18-2012
% Description    : RDSP Board Library Close
%*****
function [out] = rdspBoardLibraryClose()
    if libisloaded('RDSPD11')
        unloadlibrary RDSPD11
    end
    out=1;
end

%*****
% File Name      : rdspBoardEnableRF
% Author        : Chris Beg
% Version       : V1.0
% Date         : Feb-20-2012
% Description    : RDSP Board Enable RF Module
%*****
function [out] = rdspBoardEnableRF()
    out=calllib('RDSPD11', 'setRFEnable', 1, 1);
end

%*****
% File Name      : rdspBoardDisableRF
% Author        : Chris Beg
% Version       : V1.0
% Date         : Feb-20-2012
% Description    : RDSP Board Disable RF Module
%*****
function [out] = rdspBoardDisableRF()
    out=calllib('RDSPD11', 'setRFEnable', 1, 0);
end

%*****
% File Name      : rdspBoardSetVGAGain
% Author        : Chris Beg
% Version       : V1.0
% Date         : Apr-05-2012
% Description    : RDSP Board Set VGA Gain function wrapper
%*****
function [out] = rdspBoardSetVGAGain(gain)
    out=calllib('RDSPD11', 'setVGAGain', gain);
end

```

```

%*****
% File Name      : rdspBoardProgramPLLFrequency
% Author        : Chris Beg
% Version       : V1.0
% Date          : Feb-18-2012
% Description    : RDSP Board Program PLL Frequency Wrapper
%*****
function [out] = rdspBoardProgramPLLFrequency(frequency)
    XTAL = 8000000;
    fract = frequency / XTAL;

    [p,q] = rat(fract);

    out=calllib('RDSPD11', 'programPLLFrequency', XTAL, p, q);
end

%*****
% File Name      : rdspBoardEnableADC
% Author        : Chris Beg
% Version       : V1.0
% Date          : Feb-18-2012
% Description    : RDSP Board Enable ADC function wrapper
%*****
function [out] = rdspBoardEnableADC(channels, gain, lpf)
    out=calllib('RDSPD11', 'enableADC', channels, gain, lpf);
end

```

```

%*****
% File Name      : rdspBoardDefines
% Author        : Chris Beg
% Version       : V1.0
% Date          : Feb-20-2012
% Description    : RDSP Board Defines
%*****
% ADC channel enable selections
ADC_ENABLE_CH_A      = 0;
ADC_ENABLE_CH_AUX    = 1;
ADC_ENABLE_CH_AB     = 2;
ADC_ENABLE_CH_A_AUX  = 3;
ADC_ENABLE_CH_ABC    = 4;
ADC_ENABLE_CH_AB_AUX = 5;
ADC_ENABLE_CH_ABCD   = 6;
ADC_ENABLE_CH_ABC_AUX = 7;
ADC_ENABLE_CH_ABCDE  = 8;
ADC_ENABLE_CH_ABCD_AUX = 9;
ADC_ENABLE_CH_ABCDEF = 10;
ADC_ENABLE_CH_ABCDE_AUX = 11;

% ADC channel gain selections
ADC_GAIN_16DB      = 2;
ADC_GAIN_22DB     = 3;
ADC_GAIN_28DB     = 4;
ADC_GAIN_34DB     = 5;

% ADC channel LPF selections
ADC_LPF_DISABLED  = 15;
ADC_LPF_OP4333_FS = 8;
ADC_LPF_OP4000_FS = 9;
ADC_LPF_OP3667_FS = 10;
ADC_LPF_OP3333_FS = 11;
ADC_LPF_OP3250_FS = 0;
ADC_LPF_OP3000_FS = 12;
ADC_LPF_OP2750_FS = 2;
ADC_LPF_OP2667_FS = 13;
ADC_LPF_OP2500_FS = 3;
ADC_LPF_OP2333_FS = 14;
ADC_LPF_OP2250_FS = 4;
ADC_LPF_OP2000_FS = 5;
ADC_LPF_OP1750_FS = 6;

```

```

%*****
% File Name      : rdspBoardConfigure
% Author        : Chris Beg
% Version       : V1.0
% Date          : May-05-2012
% Description    : RDSP Board Configuration
%*****
function [result] = rdspBoardConfigure(XTAL, P, Q, VGA_GAIN)
    rdspBoardDefines;

    result      = 0;      % Assume a failure

    CHAN        = 4;
    ADC_CHAN    = ADC_ENABLE_CH_ABCD;
    ADC_GAIN    = ADC_GAIN_22DB;
    ADC_LPF     = ADC_LPF_DISABLED;
    FS          = XTAL * P / (Q*CHAN);

    openResult = rdspBoardLibraryOpen();

    if rdspBoardLibraryOpen() == 1
        disp(sprintf('DLL Library Open'))
    else
        rdspBoardLibraryClose();
        error(sprintf('Error Opening DLL Library'))
    end
    if rdspBoardEnableRF() == 1
        disp(sprintf('RF Module Enabled'))
    else
        rdspBoardLibraryClose();
        error(sprintf('Error Enabling RF Module'))
    end
    if rdspBoardSetVGAGain(VGA_GAIN) == 1
        disp(sprintf('VGA Gain set'))
    else
        rdspBoardLibraryClose();
        error(sprintf('Error Setting VGA Gain'))
    end
    if rdspBoardProgramPLLFrequency(FS*CHAN) == 1
        disp(sprintf('PLL frequency set'))
    else
        rdspBoardLibraryClose();
        error(sprintf('Error setting PLL frequency'))
    end
    if rdspBoardEnableADC(ADC_CHAN, ADC_GAIN, ADC_LPF) == 1
        disp(sprintf('ADC Enabled'))
    else
        rdspBoardLibraryClose();
        error(sprintf('Error Enabling ADC'))
    end

    rdspBoardLibraryClose();

    % If this section has been reached, everything is successful
    % Return result = 1
    result = 1;
end

```

```

%*****
% File Name      : rdspBoardCaptureData
% Author        : Chris Beg
% Version       : V1.0
% Date          : Feb-16-2012
% Description    : RDSP Board Data Capture
%*****
function [ch1, ch2, ch3, ch4, state] = rdspBoardCaptureData(N)
    rdspBoardDefines;

    VREF          = 1.024;
    LSB           = (2*VREF) / 4096;

    ch1 = [];
    ch2 = [];
    ch3 = [];
    ch4 = [];
    state = [];

    openResult = rdspBoardLibraryOpen();

    if rdspBoardLibraryOpen() == 1
        disp(sprintf('DLL Library Open'))
    else
        error(sprintf('Error Opening DLL Library'))
    end

    adcData = int16(zeros(1, 256*N));
    dacState = int16(zeros(1, 256*N));
    pADCData = libpointer('int16Ptr', adcData);
    pDACState = libpointer('int16Ptr', dacState);
    result=calllib('RDSPDll', 'receiveRealtimeADCData', N, pADCData, pDACState);
    adcData=get(pADCData, 'Value');
    dacState=get(pDACState, 'Value');

    if result==1
        state = double(dacState(4:4:end));
        ch1 = double(adcData(4:4:end)) .* LSB;
        ch2 = double(adcData(1:4:end)) .* LSB;
        ch3 = double(adcData(2:4:end)) .* LSB;
        ch4 = double(adcData(3:4:end)) .* LSB;
    end

    rdspBoardLibraryClose();
end

```

Glossary

- ADC** Analog to Digital Converter. A device which takes an analog input, and outputs a discrete time, quantized digital representation. The block is mainly characterized by the rate at which output is produced (sampling rate), and by the number of digital bits (or resolution).. [11](#), [51](#)
- DAC** Digital to analog converter. A device which takes a digital input, and outputs a voltage proportional to the quantized digital representation.. [51](#)
- DFT** Discrete Fourier transform. The discrete Fourier transform is a discrete implementation of the Fourier Transform, which performs a transformation from the time-domain into the frequency domain. This algorithm is generally heavily optimized for efficient computation on digital processors.. [37](#), [48](#)
- Doppler** An effect named after Christian Doppler who proposed that if two objects have a relative velocity, there will be an change in frequency when observing a wave or periodic event from each object. The change in frequency is related to the original frequency, and the relative velocity.. [6](#), [10](#), [17](#), [24](#), [29](#), [32](#), [34](#), [35](#), [62](#), [66](#), [67](#)
- down-chirp** A constant decrease of frequency.. [51](#)
- DSP** Digital signal processor. A digital signal processor is a microprocessor which contains hardware and an instruction set which is highly optimized for performing common tasks in signal processing algorithms.. [43](#), [45](#)
- EM** Electro-Magnetic, as in Electro-Magnetic Radiation, or Electro-Magnetic Wave. A form of energy which may be emitted or absorbed by charged particles as it travels through space. Such energy has both a magnetic field component (\vec{B}) and an electric field component (\vec{E}). Both components oscillate in phase, but perpendicular to each other as they travel at the speed of light.. [5](#)

- FM** Frequency Modulation. An information encoding scheme of which information is represented within the frequency of a sinusoidal waveform. Frequency modulation is considered a form of phase modulation [18, ch.6] .. 11, 14, 32
- FMCW** Frequency Modulation Continuous Wave. A radio system in which the transmitted wave is continuous in time and frequency. The wave is proportional in frequency to a modulating signal.. 10, 14, 19, 66, 68
- FPGA** Field programmable gate array. An FPGA is a device which emulates digital circuits through the use of a programmable gate array.. 43, 45, 49
- Hermitian** A Hermitian function is a complex function where the complex conjugate evaluated at x is equal to the original function evaluated at $-x$. I.e., $f(-x) = \text{conj}(f(x))$.. 17
- heterodyning** A process in which new frequencies are created by combining two other frequencies. This process is sometimes referred to as mixing, and is performed by computing a product or multiplication of the two input signals [18, pg.227].. 14, 15, 94
- HEV** Hybrid Electric Vehicle. 68
- IQ receiver** In communication theory, a receiver that produces both in phase and quadrature output signals, which are separated by 90 degrees.. 44
- LNA** Low Noise Amplifier. An active circuit component used to amplify signals in a radio receiver, generally placed very close to the antenna.. 10, 13
- mixer** An active circuit used to perform a multiplication function of two inputs, producing an output product. This process is also referred to as a **heterodyning** process [18, pg.227].. 13
- PA** Power Amplifier. An active circuit component used to increase the power of a signal, generally used to drive a transmitting antenna of a transmitter.. 8, 13, 14
- PM** Phase Modulation. An information encoding scheme of which information is represented within the phase of a sinusoidal waveform [18, ch.6].. 32
- RADAR** Radio Detection and Ranging. A system in which object distance, velocity and location may be determined through the use of radio waves.. 1, 10, 66

RF Radio Frequency. A term generally used to describe electro-magnetic radio waves which carry information in amplitude, frequency, or phase. The radio spectrum is considered to range from 3 kHz to 300 GHz.. [11](#), [66](#), [68](#)

RTL Register transfer level. RTL refers to a digital circuit description using a software programming language such as VHDL or Verilog. The circuit description describes the operation at a higher level by defining how states or registers are updated on a cycle to cycle basis.. [44](#), [49](#)

SI International System of Units. The SI units is the modern form of the Metric system, which describes various units used for measurements [[19](#), Appendix A].. [5](#)

SNR Signal to Noise Ratio. A ratio of signal power to noise power, usually expressed in terms of dB.. [14](#)

up-chirp A constant increase of frequency.. [19](#), [51](#)

VCO Voltage Controlled Oscillator. On oscillator for which the output frequency is in the ideal case a linear function of a control or tuning voltage.. [11](#), [13](#), [19](#), [34](#), [55](#)